Lund University

Bachelor's thesis.

Skin barrier

Extraction and characterization of Stratum Corneum lipids

Nicolas Velasquez
B. Sc. Thesis 30 hp
Division of Physical Chemistry
Lund University

Supervisor: **Emma Sparr**
Co-supervisor: **Enamul H. Mojumdar**
Examiner: **Tommy Nylander**

TABLE OF CONTENTS

ABSTRACT

The structure and dynamics of isolated Stratum Corneum lipids in different temperatures and hydration conditions was investigated using natural abundance ^{13}C NMR and X-ray scattering. In order to isolate the lipids a new extraction method was tested. The novel aspect of this method was its ability to extract more lipids from SC. This new method (referred to as Method II in-text) was further modified. The resulting method (Method III) was chosen as the method to follow during this project. These two methods were also compared (using ^{13}C NMR) to an extraction method used in a pre-study. The lipids obtained through Method III were characterized with polarization transfer solid-state NMR and wide/small angle x-ray scattering. NMR studies showed that a greater amount of lipids in a rigid state were being extracted with the new extraction method. These studies also showed that hydration has a clear effect on lipid mobility at temperatures of 32 ˚C. In the dry state there is low mobility, while upon full hydration, a fraction of lipids are in a mobile state coexist with solid lipids. SAXS studies showed that SC lipids form two types of lamellar phases, one with a lamellar repeat distance of ~144 Å in dry and hydrated conditions, while another with a repeat distance of ~71Å in dry conditions and ~68 Å in hydrated conditions. In the solid fraction of SC lipids, the hydrophobic chain adopts hexagonal packing, as detected with WAXS.

POPULAR SCIENTIFIC SUMMARY

The largest organ in our bodies is the skin. It forms a protective barrier against exogenous substances and dehydration. The barrier function is attributed to the Stratum Corneum (SC), which is the outermost layer of the skin epidermis. The main components of the SC are proteins called corneocytes (dead cells containing mainly keratin and water) and lipids. These lipids form an intercellular matrix wherein the corneocytes are embedded. This lipid matrix, which is highly ordered, consists chiefly of ceramides (CERs), free fatty acids (FFAs) and cholesterol (CHOL), in an almost equimolar ratio. Knowing how the barrier function behaves, for instance in the presence of compounds such as drugs, is extremely desirable. To do this, we studied and characterized lipids extracted from porcine SC, whose properties are highly similar to those of human SC. Their molecular mobility and structure was investigated in different conditions, such as temperature and relative humidity. Structurally, the lipids arrange themselves in periodical layers referred to as *lamellae* and are stacked parallel to the surface of the skin. Two periodicity phases have been detected, long and short. The lamellar phases also possess density, which is how tight the chains are packed together. Variations in lipid composition, temperature and hydration conditions, will alter the lipid phase behavior.

Powerful techniques used to characterize extracted lipids are ^{13}C polarization transfer solid-state NMR (PT ss-NMR) and Small/Wide X-ray scattering (S/WAXS). Both providing high resolution and sensitivity, necessary to study the microscopic properties of the intercellular lipid matrix and subsequently the skin barrier function.

ABBREVIATIONS

CER(s): Ceramide(s)
CHOL: Cholesterol
COR: Corneocyte(s)
CP: Cross-polarization
DP: Direct-polarization
FFA: Free fatty acid
INEPT: Insensitive nuclei enhanced by polarization transfer
LPP: Long periodicity phase
PT ss-NMR: Polarization transfer solid state nuclear magnetic resonance
RH: Relative humidity
SAXS: Small angle x-ray scattering
SC: Stratum Corneum
SPP: Short periodicity phase
WAXS: Wide angle x-ray scattering

1. INTRODUCTION

The skin is a crucial barrier between our body and the outside environment, protecting us from potentially harmful elements. The main barrier is located in the outermost layer of the skin and is called the stratum corneum (SC) [1]. The skin also maintains water homeostasis by providing a barrier that has low permeability to water, whose function is to minimize transepidermal water loss (TEWL).

Structurally, the skin is composed of several layers, each of which possesses a specific morphology (Figure 1.1). Beneath the SC (>25 cell layers) lies the epidermis, which can be between 50—100 μm thick, and is in turn responsible for generating the SC. The epidermis consists of three major types of cells: keratinocytes, Langerhans cells (antigen-presenting immune cells), and melanocytes (in charge of producing melanin).

Keratinocytes constitute ~95% of the cell volume and contain keratin, which plays a major structural roll in the cell. The epidermis is constructed of three layers, from the innermost to the outermost: the stratum basale (1—2 cell layers), stratum spinosum (2—7 cell layers), stratum granulosum (2—3 cell layers). Located on the basal layer are the epidermal stem cells. Upon cell division, one of these cells migrates towards the surface, undergoing differentiation as it does so, forming the corneocytes of the SC.

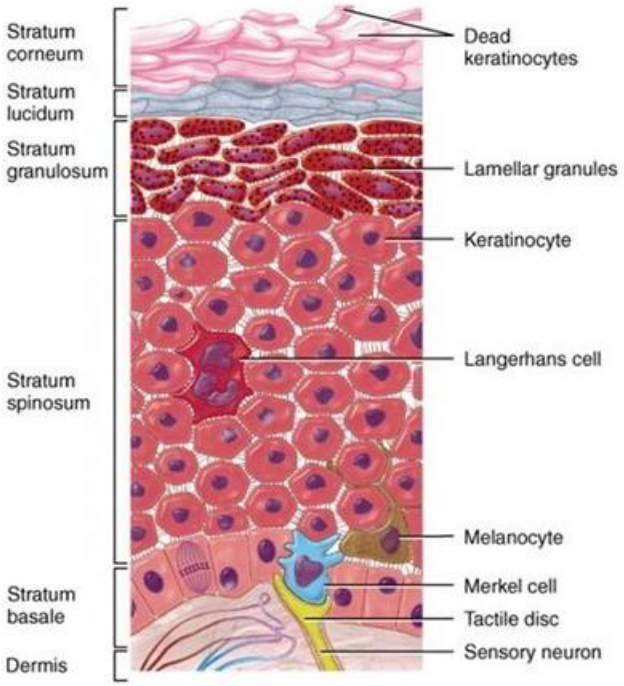

Figure 1.1: Depiction of the different layers of the epidermis and cellular structures found within.

Corneocytes are anucleated, dead flat cells containing keratin filaments and water. Water acts as a plasticizer for the keratin in corneocytes, needed to maintain their function [2]. Corneocytes are enclosed by cross-linked layers of protein, such as filaggrin, involucrin and loricrin [3], which make up the cell envelope or cornified envelope. A single layer of lipids is covalently

bound to the protein layer, the latter is often referred to as the lipid envelope, and it is in direct contact with both, hydrophobic extracellular lipids and hydrophilic corneocytes [4]. The corneocytes are embedded in a multilamellar lipid matrix that is rich in ceramides, free fatty acids and cholesterol. The majority of SC lipids are in a solid state.

The macroscopic properties of SC are sensitive to changes in RH, temperature, and several other factors. Malfunctioning of the SC can entail diseases which have their roots in disturbed keratinization or an altered lipid composition. SC is also of extreme interest regarding drug delivery systems and is a target for novel treatments of inflammatory skin diseases [5]. These and many other factors warrant a deeper understanding and knowledge of how SC components behave under different conditions.

1.1 Questions to be addressed in this project

In this thesis project, the goal is to characterize the lipids extracted from porcine SC, as well as analyze their behavior upon being subjected to different temperatures and RH. This was done using different methods, such as X-ray scattering, polarization transfer solid-state NMR (PT ss-NMR) and polarized light microscopy.

2. BACKGROUND

2.1 Main components of the Skin Barrier

2.1.1 Stratum Corneum

The SC is 2 – 10 µm thick and is composed of several layers of corneocytes, which are embedded in an extracellular lipid matrix. The corneocytes make up ca 80–90 vol % of dry SC [6]. SC lipids consists of mainly of free fatty acids (FFA), ceramides (CER) and cholesterol (CHOL) (Figure 2.1), present in a close to equimolar ratio [7]. A layer of CERs is covalently bound to the surface of the corneocytes [8]. The lipids that are bound have acyl chains that are 30—34 carbons in length. CHOL is not part of the bound lipid layer.

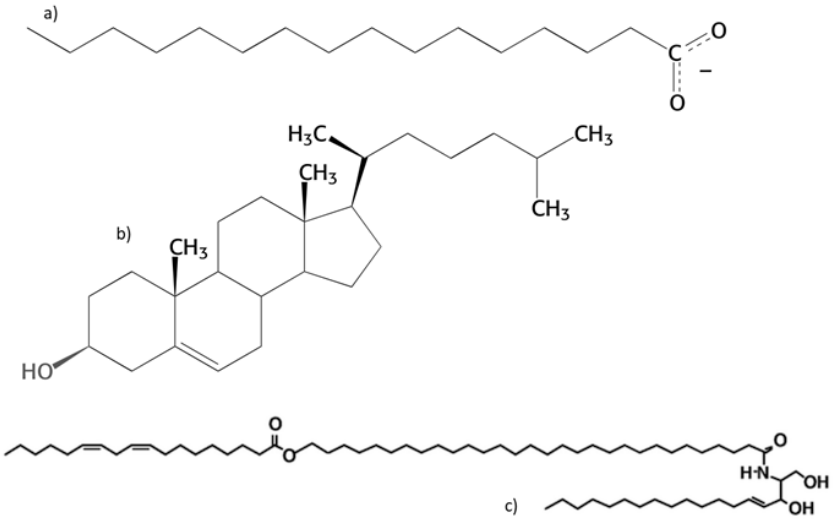

Figure 2.1: a) FFA (palmitate), b) CHOL, c) ceramide CER EOS. a) and b) Adapted from [11]; c) adapted from [13].

Structurally, the SC can be described as a brick-and-mortar model (Figure 2.2), in which the corneocytes are the bricks and the lipids are the mortar. Based on this model, transepidermal passage of substances may follow either the intracellular (through the mortar: lipid multilayers and the bricks: the corneocytes) or the extracellular (mortar: lipid multilayers) way. This extracellular lipid route is longer and more tortuous compared to the intracellular route, but can be preferred for more hydrophobic substances. For both alternative routes, the diffusing substance needs to go through the extracellular lipid matrix, as this constitutes the sole continuous pathway in the SC [3]. With this perspective, any small molecule that goes through the skin barrier must pass the extracellular lipids.

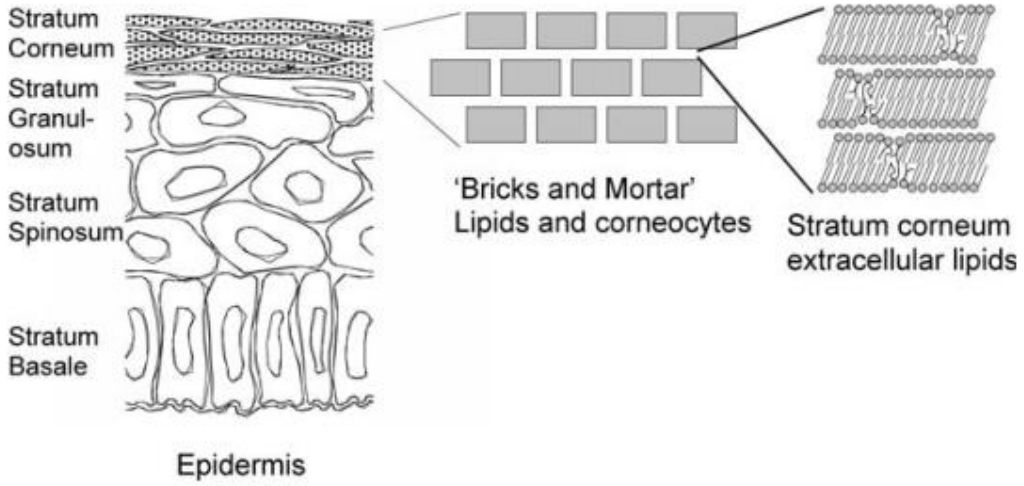

Figure 2.2: Depiction of the epidermis structure, lipid-corneocyte brick-and-mortar model and extracellular lipids. Adapted from [9].

2.1.2 Lipids

As previously mentioned, the SC contains CERs, CHOL and FFAs in approximately equimolar ratios. Together, the lipids are of highest importance for the functioning of the skin barrier. Thus, knowing their phase behavior under different types of conditions, such as temperature and hydration, can shed light about the mechanics of the skin barrier itself.

Lipids are composed of a headgroup and an acyl chain. The former is hydrophilic and can be charged or polar (water-loving), whereas the latter is hydrophobic (water-fearing) and can have different lengths and degrees of saturation. This property of matter, being hydrophilic and hydrophobic simultaneously, is referred to as amphiphilicity. It also confers them the ability to self-assemble into distinct structures with particular properties when in solution [10].

The acyl chain contains an even number of carbons, and it may be unsaturated or saturated. In most unsaturated fatty acids, the preferred configuration is *cis*, and in acyl chains with higher degrees of unsaturation, the double bonds are separated by at least one methylene group. Degree of unsaturation and chain length affect the properties of lipids; unsaturated fatty acids have lower melting points compared to saturated ones, as do shorter acyl chains. From this we can gather that shorter and unsaturated chains have the effect to promote fluidity [11]. In fatty acids the favored angle of rotation around single C-C bonds is 180˚, which occurs when the chain is

fully extended. This favored angle, or *torsion* angle is also called *trans*, followed by another favored angle of 60˚, called *gauche*.

Headgroups vary greatly from lipid to lipid, for example a ceramide is composed of a fatty acid and a sphingosine, which is in turn an amino alcohol. To date, in human SC, fourteen ceramide subclasses have been identified [12]. The ceramide headgroups and its functional groups can form hydrogen bonds with other ceramide molecules. The length of ceramide acyl chains tends to be C24-C26, while only a fraction is of a shorter length, C16-C18. C24-C26 chains are much longer than those in phospholipids found in plasma membranes. In human SC, CER1, CER4 and CER9 possess a particular molecular structure in which a linoleic acid linked via an ester to a C30-C32 ω-hydroxy fatty acid. In porcine SC this structure occurs in only one ceramide, pigCER1 [13].

In SC lipids, the fraction of FFAs is composed mainly of saturated acids. In humans the major portion of FFAs have an acyl chain length that ranges from C24:0 (39 mol%) and C26:0 (23 mol%) [14, 15]. Cholesterol sulfate, while only being present in small amounts (2-5% w/w), has an essential role in the SC desquamation process (shedding of cells from the surface) [16]. The dimensions of the acyl chains and the headgroups play an important role in self-assembly, as will be discussed later.

Lipid self-assembly

Due to the amphiphilic character of lipids, they tend to self-assemble spontaneously into distinct structures, such as lamellar, hexagonal, cubic or micellar phases (Figure 2.4). The shape they assemble into depends on the nature of the lipid (acyl chain length, headgroup), and external conditions, such as temperature, RH, pressure, pH and the presence of solutes (ions, co-surfactants). In biological membranes the most common self-assembled structure is the planar bilayer. Non-lamellar phases, e.g. bicontinuous cubic liquid crystalline phases, can also form [18].

Self-assembly is a process in which the hydrophobicity of the acyl chains works as a driving force, this is caused by the hydrophobic effect. The hydrophobic effect is the tendency of non-polar molecules (or parts of molecules), to preferentially associate with one another when present in an aqueous environment [19], to minimize contact with water. In amphiphilic molecules, the hydrophobic effect and subsequent segregation is counteracted by the repulsive interactions between the headgroups. Headgroup shape, acyl chain length and degree of saturation are important in determining the topology the aggregate adopts.

When lipids self-assemble, the curvature properties of the aggregates (Figure 2.5) is determined by how the amphiphilic molecular shape relates to the overall aggregate architecture [20]. This can relationship be expressed by the surfactant parameter (4)

$$N_s = \frac{v}{la_0} \tag{4}$$

Where v is the volume of the hydrophobic portion of the molecule, a_0 is the effective area per headgroup and l is the length of the hydrocarbon chain [20]. If the cross-section area between headgroup and acyl chain has too big a difference, such that $N_s < 0,\overline{3}$ the result would be spherical micelles. If the cross-sectional area is close to 1, then planar structures are to be expected. Lastly, if $N_s > 1$, inverted structures, such as inverted hexagonal, are the result. The surfactant parameter yields only an indicative value, as the headgroup cross-sectional area will be heavily influenced by, for example, the addition of electrolyte or an increase in amphiphile concentration [20].

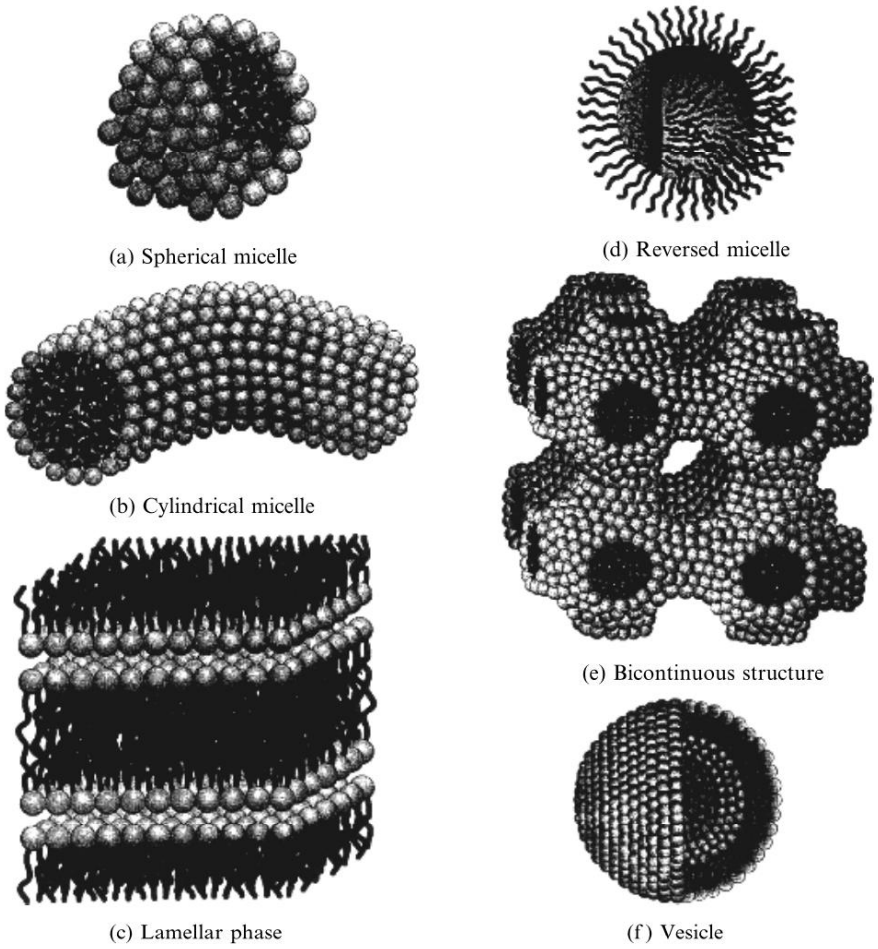

Figure 2.4: Phases that can be adopted by self-assembled structures. Adapted from [21].

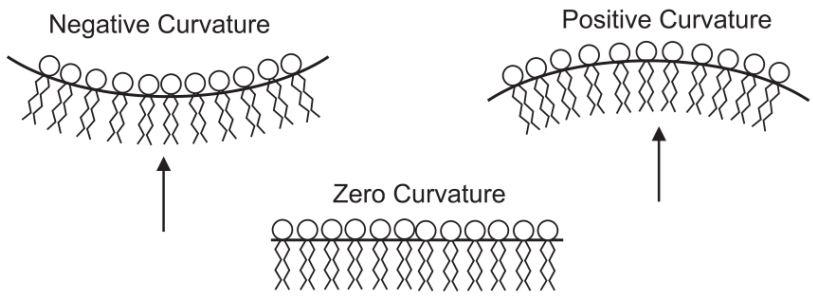

Figure 2.5: Curvature of a lipid monolayer. A reverse micelle would have a negative curvature, whereas a normal micellar structure would have a positive curvature [22]. Adapted from [23].

In the case of the SC, we will focus on lamellar structures, as they are the main self-assembly structures found in SC, forming the "mortar". The vast majority of SC lipids are in a solid crystalline or gel lamellar phase (Figure 2.6). The characteristic feature of a gel phase is that the hydrophobic chains are in a crystalline state while liquid-like solvent is present between bilayers [24].

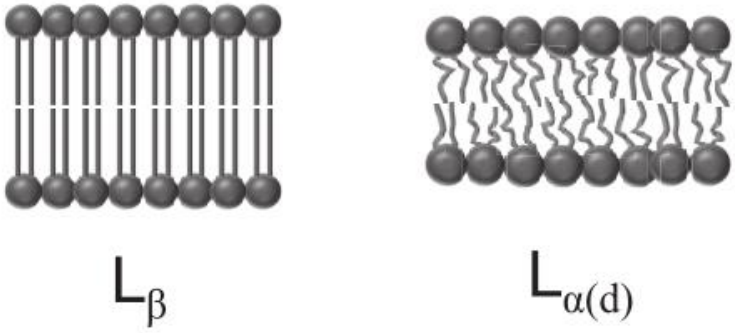

Figure 2.6: Two examples of lamellar bilayer structures. L_β = gel phase, $L_{\alpha(d)}$ = liquid crystalline disordered. Taken from [25].

The lamellar phase is composed of bilayer stacks, where the properties of each bilayer will depend on composition and external factors. To discern between different phases, it is useful to direct the attention to the acyl chain packing. Liquid crystalline lipids have disordered acyl chains, with a great portion of them in gauche conformation, and fast lateral diffusion. The hydrophobic chains of the gel phases adopt an all *trans* conformation, and commonly leads to a hexagonal chain packing with slow lateral diffusion.

To elucidate how lipids in the SC are organized, two techniques have been widely used (see section 2.2.2): Small angle x-ray scattering (SAXS) and Wide angle x-ray scattering (WAXS). SAXS gives structural insight at a larger scale, e.g. geometry of liquid crystalline phases, correspondingly WAXS does so at a smaller scale. For a lamellar phase, the SAXS pattern gives information about its repeat distance. WAXS in turn can provide information about the lateral packing of acyl chains.

Previous SAXS measurements on pig SC [17] have shown that extracellular lipids organize themselves in two different lamellar structures. Their periodicities are d = ~60 Å and d = ~130 Å. Whereas WAXS measurements revealed hexagonal lateral packing and liquid-like packing patterns with d = ~4.1 Å and d = ~4.6 Å (broad peak) respectively [13]. In human and mouse SC, an orthorhombic lateral packing has also been detected with d = ~3.7 Å and d = ~4.1 Å. This orthorhombic packing has not been observed in pig SC [13, 17]. The ~130 Å phase is commonly referred to as the *long periodicity phase* or LPP, while the ~60 Å phase is called the *short periodicity phase* or SPP (Figure 2.3) [17].

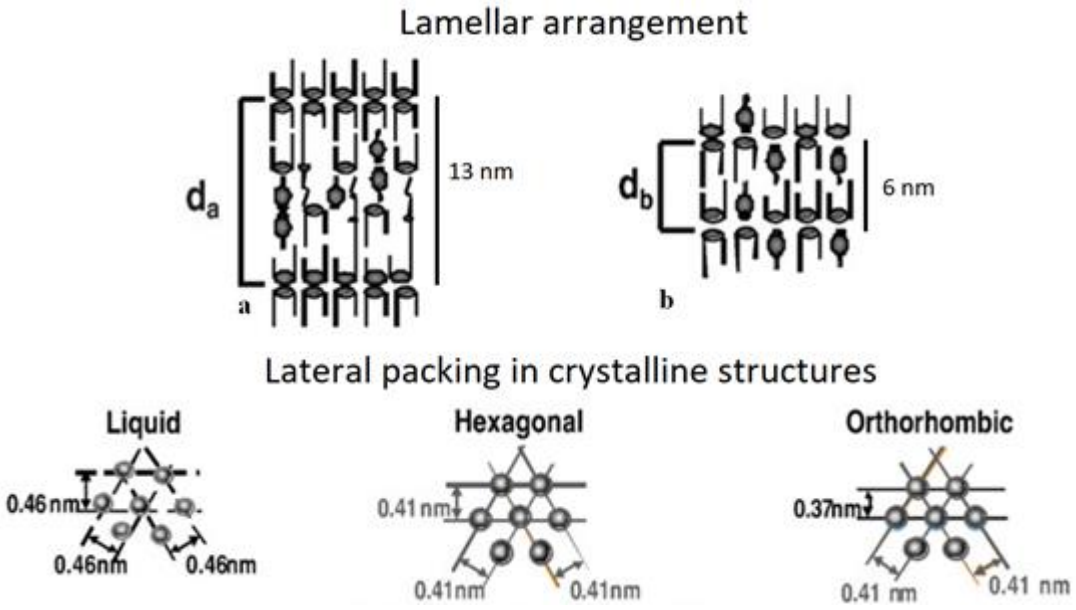

Figure 2.3: Lamellar arrangement, top: LPP (a) and SPP (b) phases. LPP would give rise to d_a spacings whereas SPP would give rise to d_b spacings in a SAXS spectrum. Lateral packing, bottom: liquid, hexagonal and orthorhombic packing. Adapted from [13].

Phase transition

When a minute alteration in composition or external factors leads to a dramatic change in structure and molecular properties, the system is said to undergo a phase transition. In self-assembled systems, there can exist solid-solid, solid-liquid or liquid-liquid transitions. For the first case, the transition can be between crystalline and gel phases, or it can be transitions between different gel phases, which involves a rearrangement of the crystalline lipid molecules [26]. The same can occur between different liquid crystalline phases, which occurs, for example, due to alterations of the bilayer curvature [26]. For a solid to liquid transition, or *main* transition, a melting of the acyl chains takes place. If the chains are long, there will consequently be a large van der Waals attraction between them, and more energy will be needed for them to melt, increasing the melting temperature T_m. For a system as complex as SC, the melting of the chains occurs over a broad range of temperatures.

Melting and other phase transitions can also be caused by a change in hydration conditions, which can be expressed as the concentration of water C_W in a sample or as the water chemical potential (μ_w), which is directly related to water activity a_{H_2O}, RH and osmotic pressure Π_{osm} as (5)

$$\Pi_{\text{osm}} = -\frac{1}{V_m}\Delta\mu_w = -\frac{RT}{V_m}\ln\left(\frac{RH}{100}\right) = f(C_W) \tag{5}$$

Where V_m is the molar volume of water, R and T are the ideal gas constant and temperature respectively and the function $f(C_W)$ relates to $\Delta\mu_w$ and water content. This function is non-trivial and depends on the system.

2.2 Characterization Techniques

2.2.1 PT ss-NMR

Atomic nuclei can possess spin angular momentum in which case they are "NMR-active". The spin can either be an α spin state or a β spin state, there is a slightly greater population of the former, and the latter has a higher energy. If a sample containing these nuclei is put in an external magnetic field B_0 and shortly exposed to a radio frequency (rf) pulse, the α nuclei can absorb the energy E and its nuclei will flip into the β spin state. When these excited nuclei return to their α state, energy that can be detected is released, resulting in a signal in the NMR spectrum.

To study the molecular mobility of a soft matter system, such as lipid bilayers, a powerful technique can be employed: polarization transfer solid-state NMR. Biological membranes are organic matter and are partly composed of carbon and hydrogen. Of these two atoms, hydrogen ^{1}H is NMR-active, and organic matter is rich in this isotope. However, the stable isotope of carbon ^{12}C is not NMR-active and will not contribute to an NMR signal [27]. Yet a carbon isotope that is NMR-active is present is ^{13}C, the problem is that it has a natural abundance of 1.1%. This can be circumvented with polarization transfer. In simplified terms, polarization from the more abundant nuclei ^{1}H is transferred to the less abundant one, ^{13}C. PT ss-NMR measurements consist of: *cross polarization* (CP), *insensitive nuclei enhanced* by *polarization transfer* (INEPT), as well as *direct polarization* (DP).

- CP: polarization transfer occurs from $^{1}H \rightarrow {}^{13}C$ by use of through-space dipolar couplings. The efficiency of the transfer depends on how the coupling is oriented in relation to the B_0 applied. For fast motion or a section with isotropic re-orientation, where dipolar couplings average out to zero, this method is inefficient. This method is effective for slow, anisotropic segments.

- INEPT: polarization is through-bond and this method will not result in signals for rigid sections of molecules and/or high anisotropic re-orientation, relaxation rate is fast, and the signal disappears before it can be registered. This method is therefore ineffective for such segments. Consequently, this experiment gives an effective enhancement of the signal for mobile segments or sections with isotropic re-orientation [28].

- DP: the resulting signal contains the resonances from all the ^{13}C nuclei in the sample and can be used as reference for the previous two methods. This experiment is a simple 90˚ pulse on the ^{13}C channel, followed by signal acquisition.

During PT ss-NMR measurements it may occur that the peaks broaden to such an extent that they might vanish completely. This is a result of the couplings between two nuclei and a phenomenon called chemical shift anisotropy (CSA). Regarding the couplings, they can be through-bond (scalar) and through-space (dipolar). In addition, these couplings can be between nuclei of the same type (homonuclear) or between different nuclei (heteronuclear). To tackle these issues, techniques such as hetero/homonuclear decoupling are used [28]. CSA occurs due

to all molecules being oriented in all directions in relation to B_0. This leads to all possible chemical shifts being superimposed with each other, giving origin to broad peaks. The latter can be dealt with by using the *magic-angle-spinning* technique (MAS). MAS entails that the sample be rotated at a specific angle of 54.7˚ in relation to B_0, which (mathematically) cancels CSA for all nuclei and gives to sharp defined peaks [29]. By combining these methods, it is possible to obtain information about the dynamics in different parts of a lipid bilayer system.

Even if characterization of lipids is the main goal of this project, the study of corneocytes and SC is also of great importance. Characterization of the latter has been performed by Björklund et al [30] and it will serve as a reference when it comes to peak assignment (Figure 2.7).

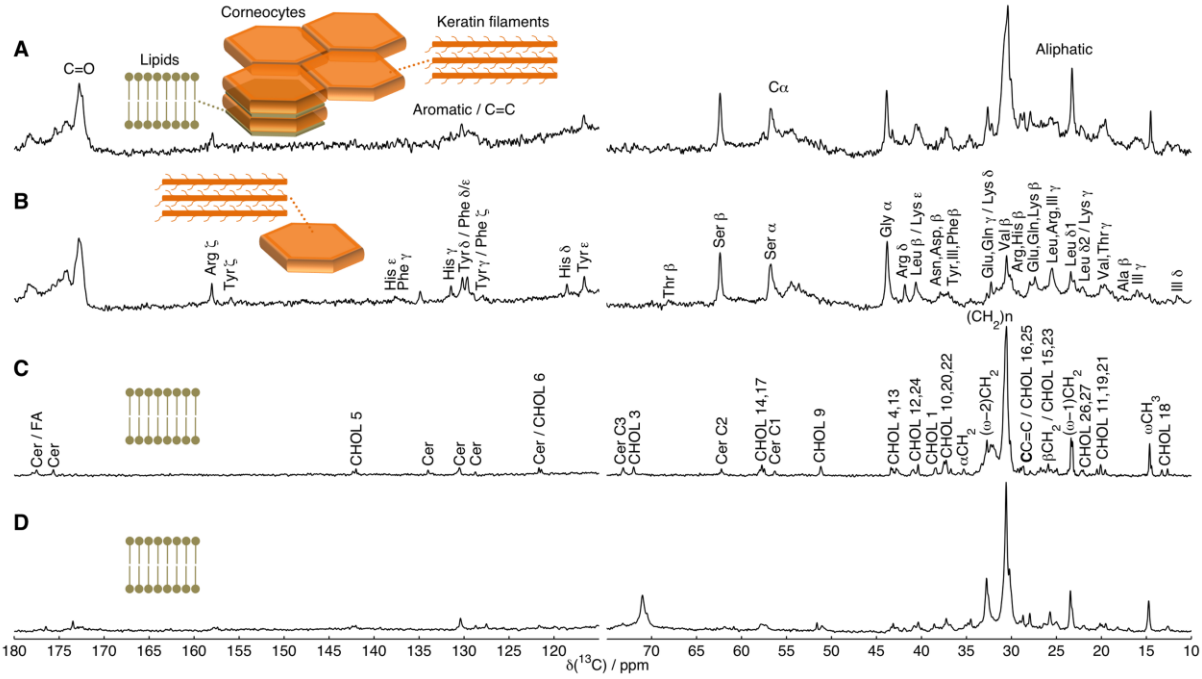

Figure 2.7: 13C DP NMR spectra of A) SC, B) isolated corneocytes C) SC model lipids D) SC extracted lipids. A) and B) were normalized at 172.8 ppm whereas A), C) and D) at 30.4-30.6 ppm. The cartoons on the upper left corner portray a scheme of how corneocytes and lipids are arranged, as well as the keratin filaments from corneocytes. Adapted from [30]. A complete list (Table A1) of the assigned peaks can also be found in [30] and is attached in the Appendix section.

2.2.2 X-ray scattering

If we consider the scattering of an x-ray by a single electron, classically the electric field of the incoming x-ray exerts a force on the electronic charge, which then accelerates and emits the scattered wave. If the wavelength of this scattered wave is the same as the incoming one, the scattering is *elastic*. Elastic x-ray scattering is the process that is taken advantage of when investigating structural properties [31].

In short, a beam of X-rays is produced by a source, this beam meets the sample, SC, lipids or corneocytes in our case, upon doing so, a fraction of the X-rays is scattered. This scattering has an intensity which is measured as a function of the scattering angle θ [32]. Let us assume our sample, composed of lipids has a repeating lamellar structure, the intensity of the scattered beam then appears as a series of peaks. This scattering intensity is plotted as a function of the scattering vector q (1)

$$q = \frac{4\,\pi \sin\theta}{\lambda} \quad (1)$$

Where λ is the wavelength. The series of peaks tell us about the periodicity of the lamellar structure, and is directly related to Braggs law (2)

$$2d \sin\theta = n\,\lambda \quad (2)$$

Where *n* is the order of the scattered peak and *d* is the repeat distance. As will be seen in the Results section, our lipid lamellar structure exhibits several peaks positioned at equidistant positions. The repeat distance can be obtained with the following equation (3)

$$d = \frac{2\,n\,\pi}{q_n} \quad (3)$$

Where q_n is the position of the n^{th} order reflection [32].

2.2.3 Polarized light microscopy

Substances in the crystalline and liquid crystalline phases have well-defined axes, inherent to their structure. As a result of this, we cannot assume that their optical properties are equal in every direction, and they may be anisotropic. The positions of the atoms within the crystalline lattice are locked, subsequently the distances between the atoms might not be equal in all directions, causing different vibrational frequencies, and a different refractive index, depending on the direction. Anisotropic optical properties are manifested through *birefringence*, a phenomenon present in, for example anisotropic crystalline structures and anisotropic liquid crystalline phases (like the lamellar phase) [33].

For the purposes of the experiments carried out during this project, this will mean that an anisotropic phase (for example, lamellar) will be displayed brightly, while an isotropic phase (micellar, reverse micellar) will be black. This can shed light on the types of phases found in a system forming within a capillary cell.

3. MATERIALS AND METHODS

3.1 Chemicals

Methanol was purchased from Merck. Chloroform, *n*-heptane, 2-propanol and KCl were purchased from VWR Chemicals. KH_2PO_4, Na_2HPO_4 and NaCl used to prepare PBS buffer were also purchased from VWR Chemicals. PBS buffer was prepared with Milli-Q water from a Merck Millipore System with a resistivity of 18 MΩ·cm at 25 °C.

3.2 Skin preparation

The lipids used throughout the experiments were extracted from the SC coming from the skin of pig ears. The ears came from Strömbecks Gårdslakt & Chark. The ears were washed, shaved

and cut into pieces adequate for dermatoming. The skin was dermatomed at a thickness of 510 µm using an Integra Padgett Model B dermatome (Plainsboro, USA). The dermatomed strips were placed on a filter paper (ø 240 mm, grade 3, Ahlstrom) and a solution of trypsin in PBS (0.2 wt%) was generously applied, soaking the filter paper. The skin was subsequently stored at 4 °C overnight and subsequently at room temperature for approximately 1 h before separation. The SC was separated from the epidermis with tweezers. It was then placed in a solution of trypsin inhibitor in PBS (0.1 wt%) and washed in four sequential beakers with Milli-Q water. SC strips were left to dry under vacuum for at least 24 h. Resulting SC was then divided into smaller pieces, which later underwent extraction. A table summarizing amounts of SC obtained can be found in the Appendix section (Table A2).

3.3 Lipid extraction

Two methods of extraction were used during the course of this project (Methods II & III). Another extraction procedure was used in a pre-study (Method I). II & III are a derivation of a procedure used by Bouwstra et al. [34], which is itself a modification of an existing protocol for extraction of lipids originally designed by Bligh & Dyer [35], in which different ratios of methanol, chloroform and water are used. The Bouwstra method was modified to use a smaller volume of solvent, otherwise the amounts of solvent needed would have been exorbitant and difficult to handle. Both procedures used will be described here. A table containing the solvent mixtures and ratios can be seen below.

Table 3.1. Solvent mixtures and ratios used during the extraction procedure. C: chloroform, M: methanol, W: water, H: heptane, I: isopropanol.

Ratio	Solvent mixture	Ratio (v:v:v)
R4	C:M:W	1:2:0.5
R5	C:M	1:1
R6	C:M	2:1
R7	H:I	1:1

Method I

SC (~1.0 g) and **R1** (400 mL) were stirred for 120 min at 37 °C. This was repeated for **R2** and **R3**. The sequence was repeated one more time with 60 min as extraction time. The SC material was then extracted overnight in methanol. The extracted lipid fraction was placed in a rotary evaporator to remove the organic solvents and dried in vacuum for at least 24 h.

Method II

SC (~1.0 g) and **R4** (400 mL) were stirred for 80 min at 40 °C. After this, the extracted lipid fraction was collected and dried under a stream of N_2 gas, in order to reduce the final volume. This procedure was then repeated for **R5-R7** (see Table 4.1). All extracted lipid fractions from different steps were combined, giving a final volume of approximately 500 mL. This volume was matched by an aq. solution of KCl (520 mL, 9.6 mM). The mixture was left to separate for two days at RT. The collected lipid fractions were filtered using a 0.45 µm filter (PTFE Minisart®). The combined filtrates were evaporated overnight under a stream of N_2 gas at RT and placed inside a vacuum oven for at least 24 h.

Method III
The main difference in this method is that no phase separation (aq. KCl solution) was performed on the extracted lipid fraction.

A table detailing the extraction procedures performed and the amounts of lipid obtained can be seen in Appendix section (Table A3).

Corneocyte treatment
After the lipids were extracted from the SC, the remaining corneocytes were at first washed Milli-Q water, in five sequential beakers, and vacuum dried for at least 24 h. It is worth noting that corneocytes showed signs of heptane contamination (see section 4.1) and had to undergo extensive washing.

3.4 Sample preparation for NMR measurements

For dry lipids, approximately 20-30 mg of the sample was put inside an NMR insert (Bruker). The lipids were dried for at least 24 h before the measurements. For fully hydrated lipids, approximately 15-30 mg were placed directly inside an NMR rotor (Bruker), and left to hydrate in excess water for at least 24 h before measuring.

All measurements were performed on a Bruker Avance AVII 500 NMR (Karlsruhe, Germany) spectrometer, with a Bruker E-free 4 mm MAS probe with a frequency of 5 kHz. ^{1}H and ^{13}C resonance frequencies are 500 and 125 MHz respectively. The spectra were recorded at 68 kHz two-pulse phase modulation (TPPM) ^{1}H decoupling with a spectral width of 250 ppm. ^{1}H and ^{13}C hard pulses were emitted at $\omega_1^{H/C}/2\pi$ = 80.6 kHz. CP measurements had a ^{13}C nutation frequency of 80 kHz while for ^{1}H it was ramped linearly from 72 to 88 kHz during a contact time of 1 ms. INEPT had delay times of τ_1 = 1.8 ms and τ_2 = 1.2 ms. 2048 scans were recorded per experiment with an acquisition and recycle delay time of 0.05 and 5 s respectively. This amounts to a total measurement time of about ~9 h for DP, CP and INEPT combined, per sample. ^{13}C chemical shift scale was externally calibrated with a methylene signal from solid α-glycine at 43.7 ppm. Experimental time domain data was processed with line broadening of 20 Hz, zero filling from 1597 to 8192 time domain points, Fourier transform, phase and baseline correction by using in-house designed MATLAB code. A temperature cycle was designed, where measurements started at 32 °C, followed by 45 °C, 68 °C, 45 °C and finally 32 °C again. The purpose was to see how temperature affected organization of the lamellar structures after being subjected to high temperatures.

For dry corneocytes samples, approximately 15 to 25 mg of dry corneocyte were placed inside an NMR insert (Bruker). For corneocytes measured at 97% RH, the sample was placed inside a desiccator with a saturated salt solution to maintain desired RH, in this case K_2SO_4 for 97% RH. The temperature was set to 32 °C, and the samples were hydrated for at least 24 h to reach stable condition.

3.5 Sample preparation for scattering measurements

For dry conditions, small amounts of lipids which had been dried for at least 24 h before the measurement, were placed between two sheets of Kapton® (DuPont™) polyimide film, and subsequently put in a tightly screwed sandwich cell. For hydrated conditions, the lipids were put in the polyimide film, and excess water was added before tightly closing the sandwich cell, which was then left hydrating for at least 24 h before measurements. The cells were then mounted on the sample holder in the X-ray machine and posteriorly measured.

SAXS and WAXS experiments were carried out using an in-house X-ray device, GANESHA 300 XL SAXS system (JJ-Xray, Denmark). The incoming beam had a wavelength λ of 1.54 Å. The distance between sample and detector was automatically adjusted based on the q range of choice, where q is the scattering vector (see section 2.2.2 eq. 1). Scattering data was collected by a PILATUS 2D photon counting detector (Dectris, Switzerland).

A temperature cycle akin to the one used for NMR experiments was used. Data was collected for approximately 30 minutes, care was taken to let the sample reach an assumed equilibrium at each temperature. Same procedure was used for hydrated samples.

3.6 Capillary sample cell design and sample preparation

The cell to be analyzed with polarized light microscopy consisted of two units. One unit was connected to an RH generator, for measurements carried out at RH other than room RH (HumiSys LF, IQI). The other unit was connected to a plastic container (reservoir). Both units were placed on a microscope slide, with the reservoir being glued to a cover-slip, and a hose glued directly to the RH generator. The sample solution was added to the reservoir and would flow to the free tip of the capillary, become exposed to air at the interface, forming a drying interfacial film.

A capillary with a cross section of 1×10 mm^2 was connected to the hose which in turn was connected to the RH generator (Figure 8, left). The capillary connected to the reservoir (Figure 8, right) had a cross section of 0.1×1 mm^2 and care was taken to ensure that it had a cleanly cut edge. Both capillaries were made of borosilicate glass (CM Scientific Ltd.). Target RH was achieved by a mixture of dry air and air saturated with water.

A Zeiss Axioplan optical microscope was used to analyze the capillary cells. The sample was put between cross-polarizers to be able to discern between isotropic (dark) and birefringent (bright) phases. Absolute length scale was calculated via AxioVision 4.8 software. Magnifications used were 10x and 20x. Capillary sample and RH-directing cells were put across each other on a microscope slide, which was subsequently put on the microscope stage. Images were collected every 15 minutes (for water-lipid solution) and 30 seconds (for pentane-lipid solution) with a color camera and the AxioVision 4.8 software.

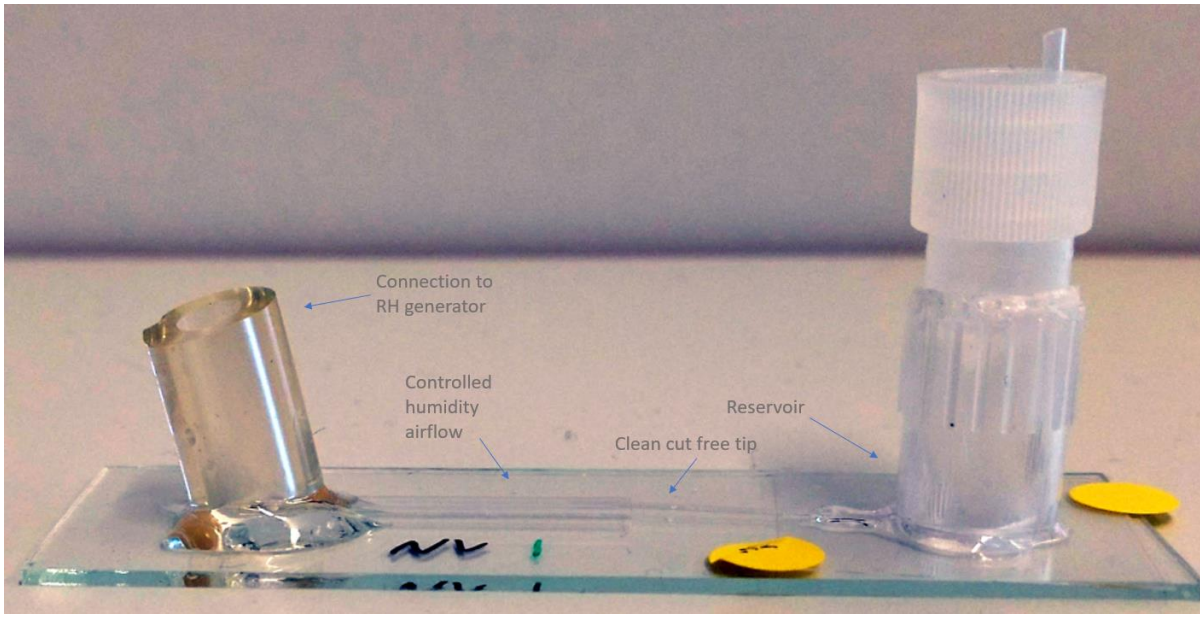

Figure 3.2: Capillary sample cell setup.

4.3 mg of extracted porcine SC lipids (via Method III) were dissolved in 3 mL Milli-Q water. The lipid solution was heated to 80 °C for 3 h, and thereafter sonicated (2 × 15 min, 75 % cycles, 90 % maximum power, 80 °C). This procedure ensured that a clear lipid solution was obtained. Other procedures including freeze-thaw cycles were tested, but which offered no advantages. The final concentration of the lipid solution used was 2.1 mM (assuming avg. molar mass of lipids 700 g/mol).

4. Results and Discussion

Lipids occupy about 15 wt% (dry) of the SC in average [36]. When an extraction procedure is performed, the lipid sample obtained should ideally consist of the extracellular portion minus the covalently bound lipid monolayer attached to the surface of the cornified envelope. This monolayer is composed mainly of non-esterified ceramides [37]. Thus, a good or efficient method implies that most of the extracellular lipids are being extracted [38], while the corneocytes contain the covalently bound rigid lipid monolayer. If the aim of the extraction is the totality of the lipids, including the covalently bound ones, then other procedures are necessary, such as saponification (procedure which makes use of strong basic agents such as NaOH or KOH) [45].

4.1 Selection of extraction method

The traditional go-to method for extraction is the Bligh & Dyer (B&D) method [35], in which different volumes of methanol, chloroform and water are mixed and used to isolate, for example, SC lipids. During this project, three methods will be compared, the first of which (Method I) was used in a pre-study, the other two (Methods II and III) were used during the course of this project. Method II is a modified B&D procedure used by Bouwstra et al. [34]. During this project, the latter was modified to use a smaller volume of solvent, otherwise the

amounts of solvent needed would have been exorbitant and difficult to handle. Table 4.1 summarizes the B&D and Methods I, II, III.

Table 4.1. Solvent mixtures and ratios used during extraction procedures. Abbreviations R1-R7 will be used in-text. C: chloroform, M: methanol, W: water, H: heptane, I: isopropanol.

1. B&D	
Solvent mixture	Ratio (v:v:v)
C:M:W	1:2:0.8
C:M:W	1:1:1

	2. Method I	
	Solvent mixture	Ratio (v:v:v)
R1	C:M	1:2
R2	C:M	1:1
R3	C:M	2:1

	3. Method II	
	Solvent mixture	Ratio (v:v:v)
R4	C:M:W	1:2:0.5
R5	C:M	1:1
R6	C:M	2:1
R7	H:I	1:1
Phase separation		

	4. Method III	
	Solvent mixture	Ratio (v:v:v)
R4	C:M:W	1:2:0.5
R5	C:M	1:1
R6	C:M	2:1
R7	H:I	1:1

Method I
SC and **R1** were stirred for 120 min at 37 °C. This was repeated for **R2** and **R3**. The sequence repeated one more time with 60 min as extraction time. The SC material was then extracted overnight in methanol. The extracted lipid fraction was placed in a rotary evaporator to remove the organic solvents and dried in vacuum for at least 24 h.

Method II
SC and **R4** were stirred for 80 min at 40 °C. After this, the extracted lipid fraction was collected and dried under a stream of N_2 gas, in order to reduce the final volume. This procedure was then repeated for **R5-R7** (see Table 4.1). All extracted lipid fractions from different steps were combined. This volume was matched by an equal volume of aq. solution with KCl (9.6 mM). The mixture was left to separate for two days at RT. The collected lipid fractions were filtered and the combined filtrates were evaporated under a stream of N_2 gas and placed inside a vacuum oven.

Method III
The main difference in this method is that no phase separation (water and KCl) was performed on the extracted lipid fraction.

A table detailing the extraction procedures performed and the amounts of lipid obtained can be seen in Appendix section (Table A3).

Figure 4.1 A shows a typical NMR spectra of porcine SC. **B** shows the NMR spectra of SC lipids in dry conditions isolated using Method I. Inspecting SC spectra we can see that CP (blue) signal is much stronger than the INEPT (red) signal, indicating a relatively rigid structure, which still contains some number of mobile segments, particularly the peaks at ~30 ppm (TG), ~23.3 ppm ($(\omega\text{-}1)CH_2$) and ~14.6 ppm (ωCH_3), which belong to lipids in the SC. These peaks are also seen in the spectra of lipids. However, in **B**, there is a relatively high INEPT signal. This leads to the following questions:

- Are we extracting extracellular solid lipids?
- Is there contamination/degradation of lipids taking place during the extraction procedure?

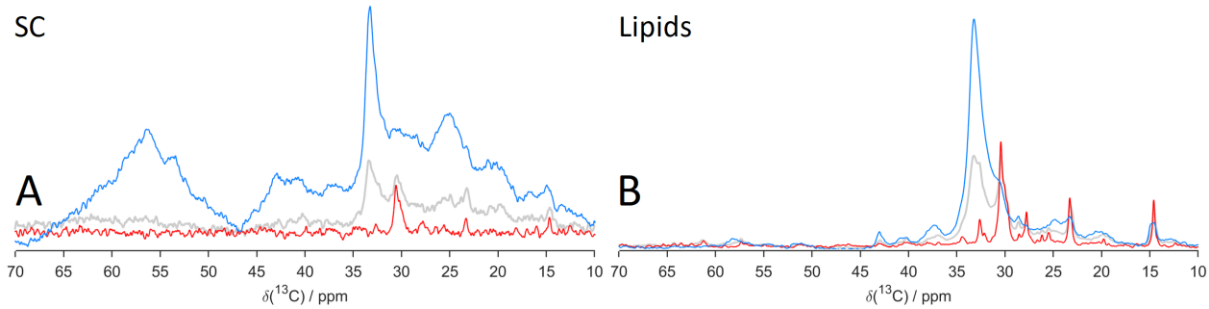

Figure 4.1: DP (grey), CP (blue) and INEPT (red) ^{13}C spectra of SC in dry conditions at 32 ˚C and extracted lipids in dry conditions at 32 ˚C from an experiment performed in 2017. Lipid extraction procedure used: Method I.

Here, we compared different extraction procedures (Methods II & III) and looked at how rigid/mobile components vary as well as look for additional peaks that can be due to contamination were used. These methods contained a more lipophilic step (Table 4.1, **R7**) compared to Method I, and the use of slightly higher temperature that may result in more efficient extraction [34].

Figure 4.2 shows the NMR spectra of lipids obtained after extracting using Methods II and III. Their INEPT to CP intensity ratios are much lower compared to those of Method I (Figure 4.1 B). This implies that the ratio between fluid and solid fractions has changed, likely suggesting that more solid lipids are being extracted using Methods II and III.

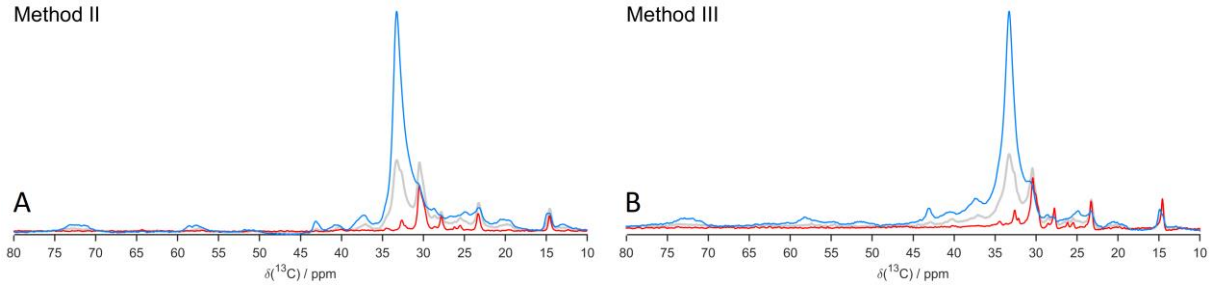

Figure 4.2: Comparison of DP, CP and INEPT ^{13}C spectra obtained from a lipids sample extracted using **A** Method II and **B** Method III (Table 4.1). Samples were measured at 32 ˚C and in dry conditions.

Inspection of the spectra shows no significant differences between Methods II and III. The samples are very similar, with a nearly identical ratio between the intensities of the CP and INEPT peaks. This suggests that Method II, which is longer and more difficult to reproduce compared to Method III, does not offer detectable advantages over Method III. Conclusively, Method III was chosen to carry out the rest of the experiments.

Lipids extracted using both methods were also analyzed with X-ray scattering. **Figure 4.3** shows SAXS and WAXS scattering patterns obtained with Methods II and III. No noticeable differences were observed, besides slightly more defined peaks corresponding to cholesterol (monohydrate and anhydrous) with Method II.

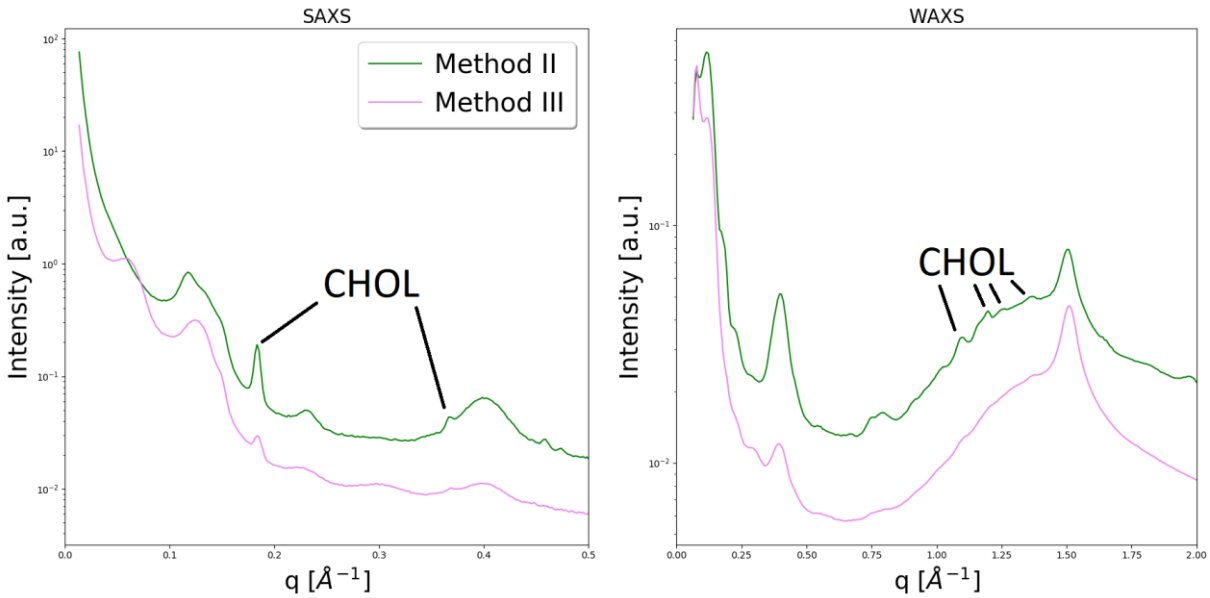

Figure 4.3: SAXS and WAXS spectra of lipids extracted using Methods II and III, at 32 ˚C in dry conditions.

Figure 4.4 shows the NMR spectra of the remaining corneocyte samples after the lipids were extracted from the SC. We would expect to see no INEPT signal contribution coming from lipids, as fluid lipids are likely extracted. To the left we observe normal looking spectra measured in dry conditions [30], showing no INEPT signal contribution coming from lipids (INEPT signals corresponding to lipids in Figure 4.2). To the right, we observe high INEPT signal at values corresponding to segments of the hydrocarbon chain: ~33 ppm and ~30ppm $(CH_2)_n$ (AT and TG respectively), ~23.3 ppm $(\omega\text{-}1)CH_2$, ~14.6 ppm ωCH_3. This posed a problem as the heptane used in the extraction procedure could also give rise to peaks at the same chemical shifts (see Appendix section for ^{13}C NMR spectra of heptane Figure A1).

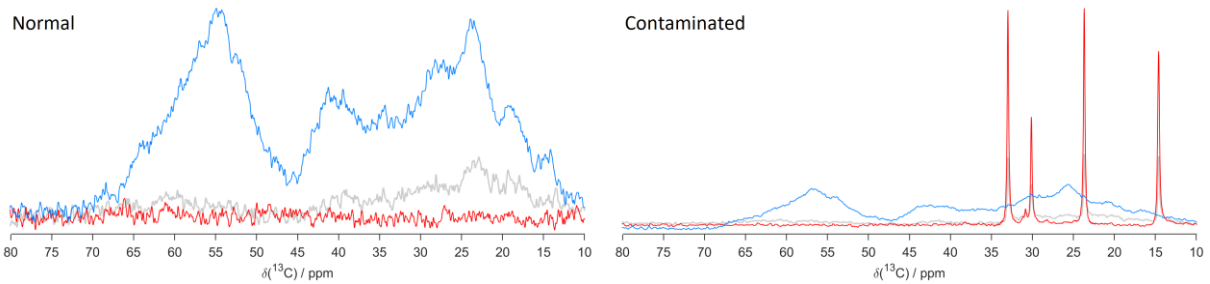

Figure 4.4: Comparison of DP, CP and INEPT ^{13}C spectra obtained from a corneocytes sample, measured at 32 °C in dry conditions.

This meant that we could not analyze corneocyte samples directly unless they had been washed extensively. This was the main drawback of Methods II & III. A figure with the NMR spectra of washed corneocytes can be seen in the Appendix section (Figure A2).

Conclusion

Method II was adopted as a starting extraction procedure for this project. It was modified, giving origin to Method III. Method II incorporated a phase separation step that added 3-4 days to the extraction process, and more chance for contamination. Method III skipped this step

altogether. After analyzing the samples obtained from Methods II and III with PT ss-NMR and X-ray scattering, it was found that they are hardly distinguishable, yet both differ from Method I . All further characterization experiments utilized Method III.

4.2 Rebuilding NMR spectra from extracted SC lipids & isolated corneocytes

In broad terms, the SC system is composed of lipids and corneocytes. Lipid extraction leads to the isolation of corneocytes. Perfect extraction would entail that 100% of the lipids have been extracted from the SC, while the remaining product would only consist of corneocytes. However, such a complete extraction of SC lipids cannot occur unless we use harsher methods to remove the covalently bound lipid monolayer. In other words, methods based on organic solvent extraction, can only extract extracellular lipids, which are also the lipids components considered most relevant for SC barrier function.

There is always risk for introduction of contaminants or breakage of SC molecular components during an extraction procedure. This would likely influence self-assembly structures. It is also possible that the separation of extracellular lipids from the corneocytes environment would influence their state. To test this, an analysis was made where the CP and INEPT ^{13}C NMR spectra from intact SC was compared to the corresponding ^{13}C NMR spectra reconstructed from a linear combination of CP and INEPT spectra from extracted lipids and isolated corneocytes. Doing so, can tell us about the quality of the sample after extraction. It can also tell us about any contaminants presents.

In the 55—57 ppm spectral regime there is only CP signal (and no INEPT signal) contribution for the SC sample mainly originating from rigid amino acids (Figure 4.1, A). Correspondingly, there is CP signal contribution for the corneocyte sample in the same spectral regime (Figure 4.4, left). Contrariwise, no/very low CP signal contribution is detected at the same ppm regime coming from the lipid sample (Figure 4.2 A, B).

The linear combination is represented by the following equations (6, 7)

$$\mathrm{CP}_{SC\ Rec} = a\ CP_{COR} + b\ CP_{LIP} \quad \textbf{(6)}$$

$$\mathrm{INEPT}_{SC\ Rec} = a\ INEPT_{COR} + b\ INEPT_{LIP} \quad \textbf{(7)}$$

Where the constants *a* and *b* are the same in both equations. Constant *a* is obtained by adjusting CP_{COR} to $\mathrm{CP}_{SC\ Exp}$ at the 55—57 ppm spectral regime. The lipid spectra were then added, and constant *b* was adjusted to make a good fit of the CP spectra for the whole spectral regime. Upon completion, the same constants *a* and *b* were used to calculate the reconstructed $\mathrm{INEPT}_{SC\ Rec}$, according to (7), this was compared to experimental data from $\mathrm{INEPT}_{SC\ Exp}$.

Figure 4.6 shows the plotting of experimental (solid lines) vs reconstructed (dotted lines) SC CP INEPT ^{13}C spectra for lipids extracted using methods II and III. As this is a qualitative exercise, we cannot directly compare the two methods. What we can conclude from the

analysis, however, is that we can reproduce the SC ^{13}C NMR spectra from the its two main components' -lipids and corneocytes- corresponding spectra. In other words, their molecular dynamics properties, as revealed by PT ss-NMR, are close to *additive*. The molecular dynamics of corneocyte components and the lipids does not change in any significant way, whether they are analyzed as constituents of the intact SC or as isolated fractions after extraction.

Detection of contaminants

The comparison between the reconstructed and experimental spectra can also be used to check for any possible contaminants that may have entered the organic volume during the extraction procedure. Expected contaminants include, squalene, unsaturated fatty acids, phosphatidylcholine and triglycerides (part of the oily layer covering the skin, called sebum lipids) [44], amongst others. If an extraneous substance found its way towards the lipids sample, it would appear on the reconstructed ^{13}C NMR spectra but not on the experimental one. In particular, small mobile molecules would be visible in the INEPT spectra. As we can appreciate in Figure 4.6 A—B (upfield regime), C—D (downfield regime), no such peaks are visible. We can say that there are no detectable levels of contaminants, at least measuring SC sample in dry conditions.

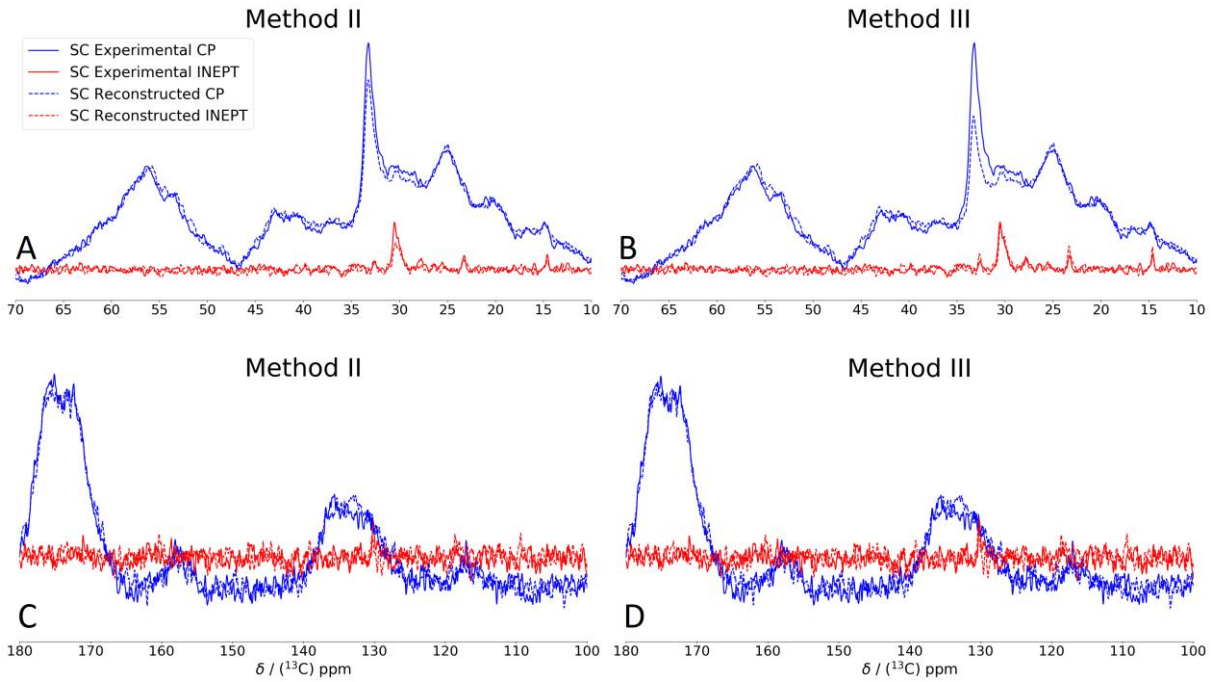

Figure 4.6: Reconstructed vs Experimental SC spectra (only CP and INEPT ^{13}C are plotted). All samples were measured at 32 ˚C and in dry conditions.

Conclusion

The linear combination of CP and INEPT ^{13}C NMR spectra from extracted components into the reconstructed spectra is useful to analyze the quality of the extracted lipid sample. It also revealed that the properties of lipids and corneocytes are close to additive. The exercise served as a tool to check for possible contaminants in the lipids sample, none of which could be confirmed using PT ss-NMR.

4.3 Lipid characterization

4.3.1 Structural features of extracted lipids observed through X-ray scattering

Figure 4.7 and **Table 4.1** summarize the data obtained by S/WAXS measurements. The low intensity of the peaks could be due to a low signal-to-noise ratio likely caused to the small amount of sample and insufficient scan time. Extracted lipids underwent a temperature cycle in both dry and fully hydrated conditions. Several poorly resolved peaks become clearer only after the heating cycle, which can be related to annealing of the solid bilayer structures after the melting step. For this reason, we will focus on the maximum temperature (when the sample is melted) and downscan temperatures (45 to 32 ˚C).

SAXS Dry conditions

Figure 4.7 A shows the SAXS scattering profiles of extracted lipids in dry conditions which underwent a temperature cycle. Data presented here corresponds to one experiment

32 ˚C Start cycle & 45 ˚C upscan

The majority of peaks in these temperatures are too broad and unresolved to be assigned. However, peaks at ~34.3 Å and ~17.1 Å (Figure 4.7 A, *) have been shown to correspond to CHOL microcrystals [17].

68 ˚C Maximum temperature

At 68 °C, most peaks disappear. Two broad reflections remain. A noticeable broad peak at ~42.6 Å and a low intensity peak at ~20.0 Å. The peaks attributed to CHOL microcrystals are not present, indicating a higher solubility of cholesterol in the lipid melt [17]. The ~42.6 Å peak suggests the presence of an isotropic structure, possibly small oil droplets. The presence of the ~20.0 Å peak possibly indicates that not all of the lipids had melted at this temperature.

45 ˚C Downscan

Here we observe the appearance of well-defined higher order peaks. A peak at ~144.1 Å could correspond to LPP1 (1^{st} order reflection). The ~72.2 Å peak could be assigned to LPP2 (2^{nd} order reflection) and/or SPP1 (1^{st} order reflection), while the peak at ~48.9 Å could be attributed to LPP3 (3^{rd} order reflection). The ~36.5 Å and ~24.1 Å peaks can be assigned to SPP2 (2^{nd} order reflection) and SPP3 (3^{rd} order reflection) respectively. The peak at ~29.2 Å is now more defined, consequently it can be assigned to LPP5 (5^{th} order reflection). CHOL reflections do not reappear when the temperature is decreased, suggesting that CHOL becomes a part of the lamellar structures after it has dissolved in the lipid melt at the highest temperature [17].

32 ˚C End cycle

At 32 ˚C the sample gives very similar patterns as the samples at 45 ˚C, although the majority of the peaks have shifted to a greater *q* value while the peaks at ~144.1 Å and ~48.9 Å have not shifted. When the sample has cooled down, there are four identifiable LPP orders (LPP1,2,3,5), and two for SPP (1,2). CHOL reflections are not visible at the end of the cycle at 32 ˚C, suggesting that it has become part of the lamellar structures after dissolving in the lipid melt at 68 ˚C [17].

Table 4.1. Summary of LPP, SPP, CHOL, hexagonal, liquid lateral packing peaks assigned in SAXS and WAXS for dry and fully hydrated conditions. **LPP** = long periodicity phase. **SPP** = short periodicity phase. **C** = CHOL. **Hex** = hexagonal lateral packing. **Liq** = liquid packing. **+** = present. **-** = not present/unclear. **Ord** = higher order reflections. Temperature in C˚. Peak distances in Å. The Bragg reflections attributed to LPP and SPP were assigned by fitting lines parallel to the reference peak (3rd order reflection in the case of LPP and 1st order reflection in the case of SPP), a compromise between the peak found by the parallel line and the peak found by the peak-finding algorithm. Parallel lines were not featured in the in-text Figure for clarity (Figure can be seen in Appendix section, Figures A5 & 6). Asterisks next to reflection indicates tentative assignments.

T	SAXS										WAXS					
	Dry					Full Hydration					Dry			Full Hydration		
	LPP	Ord	SPP	Ord	C	LPP	Ord	SPP	Ord	C	Hex	Liq	C	Hex	Liq	C
32	-	-	-	-	+	-	-	-	-	-	4.16	-	+	4.16	-	-
45	-	-	-	-	+	-	-	-	-	-	4.18	-	+	4.20	-	-
68	-	-	-	-	-	-	-	-	-	-	-	4.61	-	-	4.68	-
45	144.1	1,2,3,5	72.2	I,II	-	132.6	1,2,3,5	67.8	I,III	-	4.16	-	-	4.20	-	-
35	144.1	1,2,3,5	70.7	I,II	-	144.1	1,2,3,5*	67.8	I,III*	-	4.13	-	-	4.16	-	-

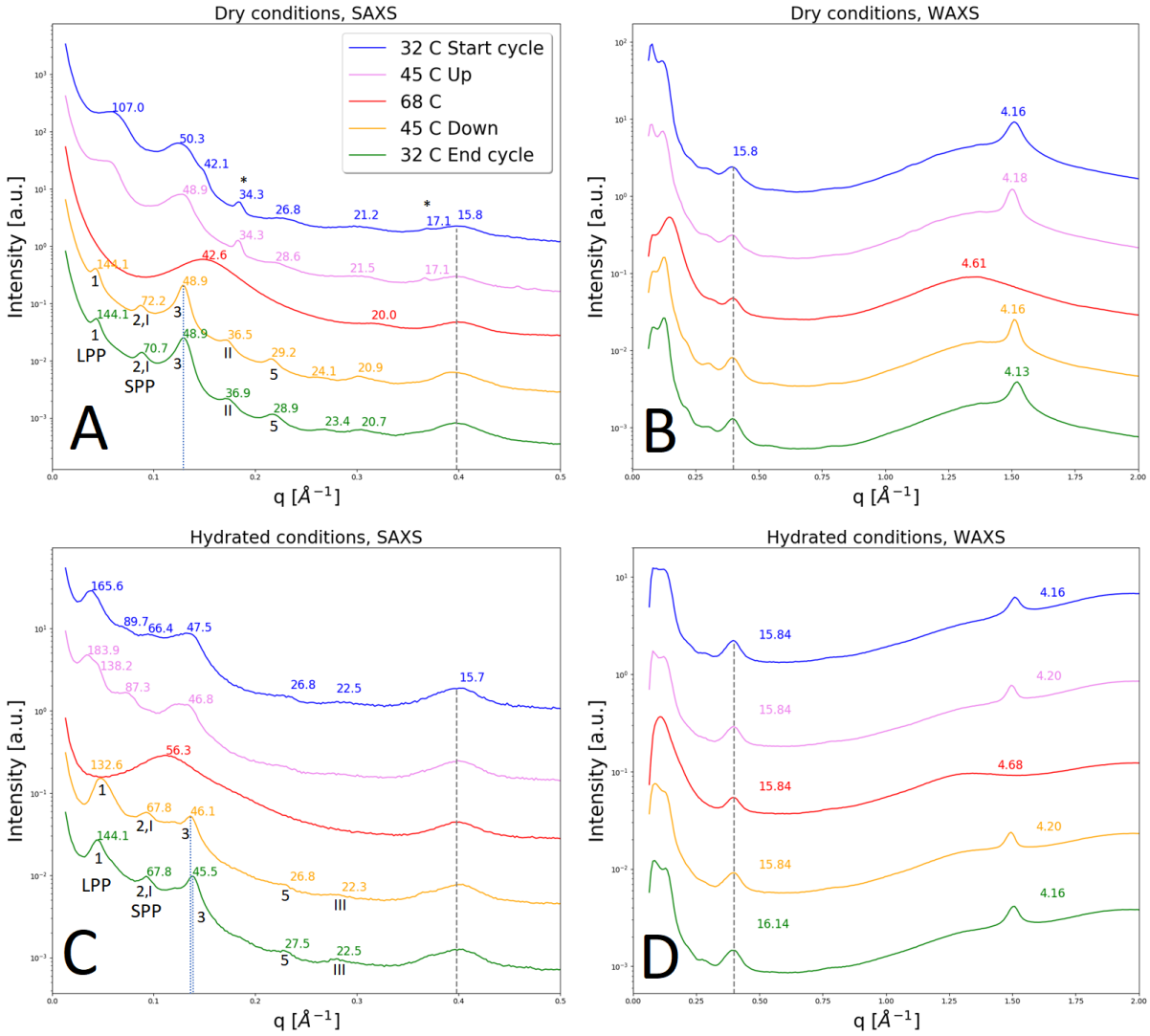

Figure 4.7: SAXS pattern of extracted lipids in dry conditions. Intensities have been scaled in order to present a better view of each curve. Peaks at ~15.7—15.8 Å (dotted grey line) correspond to the Kapton film background (see Appendix section for background spectra Figures A3, A4). Arabic numerals in the SAXS profile dry conditions, indicate the different diffraction orders attributed to the *LPP* with a repeat distance of **A**: 144.1 Å (45,32 °C); **C**: 132.6 Å (45 °C), 144.1 Å (32 °C). Roman numerals indicate the different diffraction orders attributed to the *SPP* with a repeat distance of **A**: 72.2 Å (45 °C), 70.7 Å (32 °C); **C**: 67.8 Å (45, 32 °C). In-text, these will be referred to as LPP1, SPPI, etc. Asterisks indicate peaks attributed to CHOL. Dotted blue line (LPP 3rd order) indicates the strongest peak detected used as reference to fit the remaining orders.

WAXS Dry conditions

Figure 4.7 B. At all temperatures, except 68 ˚C, there is the peak characteristic for hexagonal chain packing [17] in the narrow range of ~4.13—4.18 Å. Upon reaching 68 °C, we observe a phase change where the hexagonal chain packing peak disappears and is replaced by a broad bump at ~4.61 Å. This bump is characteristic for liquid packing, indicative of high rotational disorder of the hydrocarbon chains [13].

Anhydrous crystalline CHOL, which has also been characterized in previous X-ray diffraction studies [17], is almost imperceptible during these experiments and only perceived as extremely low intensity bumps sloping off the left side of the hexagonal chain packing peak (**B**, 32 °C start cycle and 45 °C upscan). These bumps at ~4.55 Å, ~5.22 Å, ~5.77 Å and ~6.23 Å are visible only at the beginning of the cycle between 32 °C and 45 °C. When decreasing the temperature from 68 ˚C, only the smallest of these bumps can be perceived at ~4.56 Å, suggesting that most of the CHOL has been dissolved into lipid lamellar phases. That anhydrous CHOL disappears from the spectra at 68 ˚C suggests that CHOL dissolves in the lipid mixture, possibly due to the liquid state at higher temperatures [17].

Summary dry conditions

Dry lipids at the beginning of the cycle give rise to Bragg reflections, although, higher order reflections seen as several broad peaks, cannot be resolved. However, after heating to 68 ˚C and cooling down, more well-defined peaks could be assigned as higher order reflections of LPP and SPP. Their spacings are LPP at ~144.1 Å and SPP at ~70.7 Å, as detected at the end of the temperature cycle. These values are slightly larger compared to corresponding values found in the literature [17, 40, 46]. These studies report estimated values for LPP of ~130 Å and for SPP of ~60 Å, for porcine, human and murine SC lipids. The difference may be attributed to the types of samples (measurements of intact SC), experimental conditions (maximum temperatures of up to 120 ˚C in some cases [17]) and sample preparation methods (SC sample pulverization [46]), as well as extraction procedures (unmodified B&D methods [46]). Crystalline CHOL present at 32 ˚C and 45 ˚C melts and is incorporated in the lamellar structure, where it may influence the repeat distances.

SAXS fully hydrated conditions

Figure 4.7 C shows scattering profile of fully hydrated lipids undergoing the temperature cycle.

32 ˚C Start cycle & 45 ˚C upscan

As was the case with lipids in dry conditions, the majority of peaks here are too broad and unresolved to be assigned, particularly in the low *q* region. Peaks that correspond to CHOL microcrystals are not visible.

68 ˚C Maximum temperature

Reaching 68 °C shows all peaks disappearing except for one noticeable broad peak at ~56.3 Å, which suggests the formation of an isotropic structure, possibly small lipids encapsulating small

water drop in a reverse micellar type of structure. The lamellar phase has disappeared at this high temperature, as indicated by the disappearance of lamellar reflections.

45 ˚C Downscan

A defined peak at ~132.6 Å has appeared, possibly corresponding to LPP1, followed by a peak at ~67.8 Å, which likely corresponds to SPP1 and/or LPP2. A peak at ~46.1 Å is now resolved and can be attributed to LPP3. The last two broad bumps are at ~26.8 Å and ~22.3 Å and could likely be attributed to LPP5 and SPP3 (3rd order reflection) respectively.

32 ˚C End cycle

The ~132.6 Å peak shifted to a lower *q* value, while the peak at ~67.8 Å (SPP1/LPP2) remains close to unaltered. The peak at ~46.1 Å shifted to a higher *q* value. Two broad bumps at ~27.5 Å and ~22.5 Å are visible and could be attributed to LPP5 and SPP3 respectively. However, due to the low intensity and poor resolution, these assignments must be considered as tentative until additional experiments can be carried out.

It is interesting to notice that the LPP has the same position as the sample in dry conditions (~144.1 Å), but at 45 ˚C, the position of the LPP in fully hydrated conditions differs by ~12 Å (~132.6 Å).

WAXS Fully hydrated conditions

Figure 4.7 D shows the WAXS scattering profile for lipids in fully hydrated conditions. Here there are no visible or barely imperceptible bumps belonging to CHOL. The hexagonal chain packing peak at around ~4.16—4.20 Å can be seen at all temperatures except 68 °C. At 68 °C we see a broad bump indicative of a liquid packing of the hydrophobic chains.

Summary fully hydrated conditions

In fully hydrated conditions, the lipids at 32 °C and 45 °C give rise to broad and unresolved peaks, especially in the low *q* region. It is only after heating to 68 °C and cooling down that we can observe some degree of resolution in the Bragg reflections. When the lipids have cooled down, the LPP and SPP have appeared as more defined reflections with values of LPP ~144.1 Å and SPP ~67.8 Å, as measured at 32 °C. Peaks corresponding to CHOL microcrystals are not observed in fully hydrated conditions.

Dry vs Fully hydrated conditions

Figure 4.8 shows a direct comparison of the scattering profiles obtained at 68 °C, 45 °C and 32 °C. Figure 4.8 **A** shows the SAXS spectra at the maximum temperature. In dry conditions there are two broad bumps remaining, ~42.6 Å and ~20.0 Å. Of these two, the former may correspond to an isotropic structure (oil droplet). When fully hydrating the sample, this peak shifts to a lower *q* value, with a spacing of ~56.3 Å. This broad bump may also correspond to an isotropic structure (reverse micelles). A bump at ~42.6 Å has been previously reported for model lipid mixtures prepared with human and pig ceramides in dry conditions and appears at elevated temperatures above 53 ˚C [41].

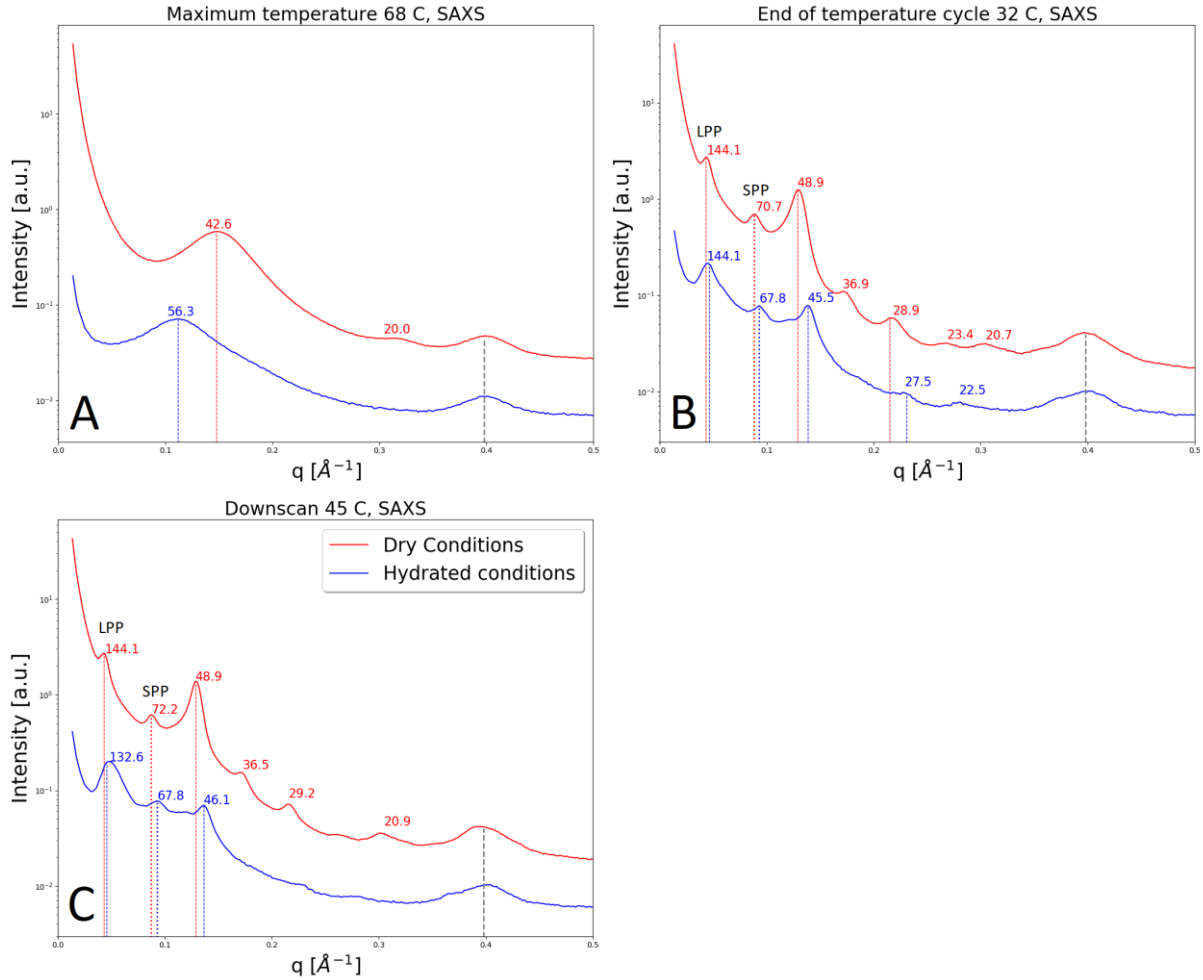

Figure 4.8: SAXS pattern of lipid samples in dry vs fully hydrated conditions. **A** = 68 °C. **B** = 32 °C (end cycle). **C** = 45 °C (downscan). Intensities have been scaled in order to present a better view of each curve. Dashed lines correspond to LPP higher orders. Dotted lines correspond to SPP (only showing the SPPI for clarity). Dashed grey line corresponds to the Kapton film background peak.

Currently we have no explanation for the bump at 20 ˚C observed in dry conditions, other than the possibility that not all lipids have melted at this temperature.

Figure 4.8 **B** shows the SAXS spectra at 32 ˚C. After cooling down from 68 ˚C, Bragg reflections are more defined. The peaks corresponding to LPP1 show a lamellar repeat distance of ~144.1 Å for both dry and fully hydrated conditions, indicating that there are no signs of swelling in this phase. Peaks attributed to SPP1 in dry conditions (~70.7 Å dry, ~67.8 Å fully hydrated) show sign of deswelling of this lamellar phase. Possible explanations for the deswelling are effects have their origin in the sample not reaching equilibrium. Deswelling may also reflect change in lipid packing in the bilayer: a higher fraction of chains in the fluid state would lead to a thinner bilayer, which could in turn lead to a smaller lamellar repeat distance. To confirm this effect, the experiments should be repeated.

Figure 4.8 **C** shows the SAXS spectra at 45 ˚C. The peaks corresponding to LPP1 (~144.1 Å dry, ~132.6 Å fully hydrated), indeed show signs of deswelling of the LPP with hydration. It is here noted that the spacings for the LPP phase were measured to ~144 Å for all other

temperatures and hydration conditions. The same is seen for SPP1 (~72.2 Å dry, ~67.8 Å fully hydrated). The peaks corresponding to LPP3 (~48.9 Å dry, ~46.1 Å fully hydrated) display the same trend as both LPP1 and SPP1.

Conclusion

Scattering studies were done with lipids extracted from pig SC. Lipids were analyzed as a function of hydration and temperature. Lipids were measured with no pre-treatment. They underwent a temperature cycle in dry and fully hydrated conditions. At the 32 ˚C start cycle and 45 ˚C upscan, in both conditions, Bragg reflections were broad and of poor resolution. After heating to 68 ˚C and cooling down, well-defined peaks with several higher order reflections could be assigned to LPP and SPP (Figure 4.7, Table 4.1).

At 68 ˚C in dry conditions an isotropic structure has likely formed, possibly an oil droplet. In fully hydrated conditions there is also an indication of an isotropic structure, likely a reverse micelle. At 32 ˚C end of cycle, LPP and SPP could be observed, with spacings of ~144.1 Å for LPP and ~70.7 Å for SPP, in dry conditions. In fully hydrated conditions the spacings for LPP and SPP were ~144.1 Å and ~67.8 Å respectively. LPP and SPP values found in the literature [17, 40, 46] report estimated values of ~130.0 Å and ~60.0 Å respectively, for porcine, human and murine SC lipids. The differences observed in this study may indeed be attributed to the types of samples (measurements of intact SC), experimental conditions (maximum temperatures of up to 120 ˚C in some cases [17]) and sample preparation methods (SC sample pulverization [46]), as well as extraction procedures (unmodified B&D methods [46]). These differences in experimental conditions, as well as sample preparation and origin could in turn lead to a different molecular composition of the lipids, which could likely explain the LPP & SPP values observed in this study.

CHOL was observed in SAXS, dry conditions, at 32 ˚C and 45 ˚C. When reaching 68 ˚C, CHOL peaks are no longer visible, suggesting higher solubility in the lipid mixture. When the temperature decreases, CHOL reflections do not reappear, indicating that it has become part of the lamellar phase when the sample is cooled down from the maximum temperature. The incorporation of CHOL in the lamellar phase may influence the repeat distances [48].

4.3.2 Molecular mobility of extracted lipids as revealed from PT ss-NMR

The effect of temperature and hydration on the molecular mobility of extracted lipids was investigated using natural abundance ^{13}C PT ss-NMR. Analyzing the CP and INEPT signals in relation to DP signals, we can obtain information as to the mobility and rigidity of the lipids sample. If only CP signal is detected, then that molecular segment can be described as rigid. Conversely if only INEPT signal is observed, it indicates that the molecular segment is mobile and isotropic. A fluid and anisotropic segment gives rise to both INEPT and CP signals. The samples underwent the same temperature cycle in both dry and fully hydrated conditions, as the samples analyzed with X-ray scattering.

Figure 4.9 shows the standard numbering for CHOL lipid carbons displayed in the NMR spectra.

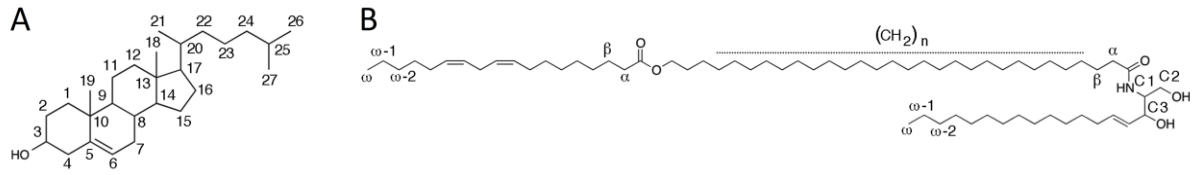

Figure 4.9: Standard numbering of A CHOL carbons and labels of B relevant lipid carbons, illustrated here with a ceramide lipid (CER EOS). Taken from [42].

The data obtained will be divided in three different groups, coming from different parts of the lipid system. We will focus on the 68 °C, 45 °C and 32 °C, since as observed in X-ray scattering results, it is here where the interesting features are found. However, the 32 °C and 45 °C temperatures will be described briefly. The different groups are:

1) Acyl chains with peaks at ~33-34 ppm (AT), ~30 ppm (TG), ~23.3 ppm ($(\omega\text{-}1)CH_2$) and ~14.6 ppm (ωCH_3)**.**

2) CHOL peaks, spread throughout the spectra (downfield → upfield order: CHOL C3, C14, C17, C9, C13, C24, C10, C20, C22, C16, C25, C15, C23, C18).

3) Ceramide peaks: headgroup (CER C1, C2, C3), chain segments close to the headgroup (αCH_2, βCH_2), conjugated double bonds and adjacent (CC=C, C=C).

Figure 4.10 shows the NMR spectra of extracted lipids subjected to the temperature cycle in dry and fully hydrated conditions. **Figure 4.11** shows a magnified image in the 80—50 ppm regime. **Figure 4.12** shows the downfield spectral regime, where CER peaks are found.

Lipids in dry conditions

32 ˚C Start cycle & 45 ˚C upscan

Figures 4.10, **4.11**, **4.12 A** and **C** show the lipids at 32 ˚C and 45 ˚C. **1)** The AT peak is predominant, showing high intensity CP signal, indicating that the CH_2 groups of the acyl chains are in a rigid AT conformation. There is INEPT signal contribution from acyl chain peaks, indicating that at this temperature, a fraction of them are in a fluid state. **2)** CHOL peaks all display CP signal and no INEPT signal contribution, with few exceptions. **3)** CER headgroup carbons and CER carbons in the chain segments close to the headgroup display CP signal contribution (Figures 4.11 A, C). In the downfield region (Figure 4.12 A), CER peaks corresponding to conjugated double bonds, which are mainly found in ceramides [47] display mostly INEPT contribution. Taken together this implies that in the same molecules there are both mobile and rigid segments, as has been previously described for a model mixture of CER:FFA:CHOL [47].

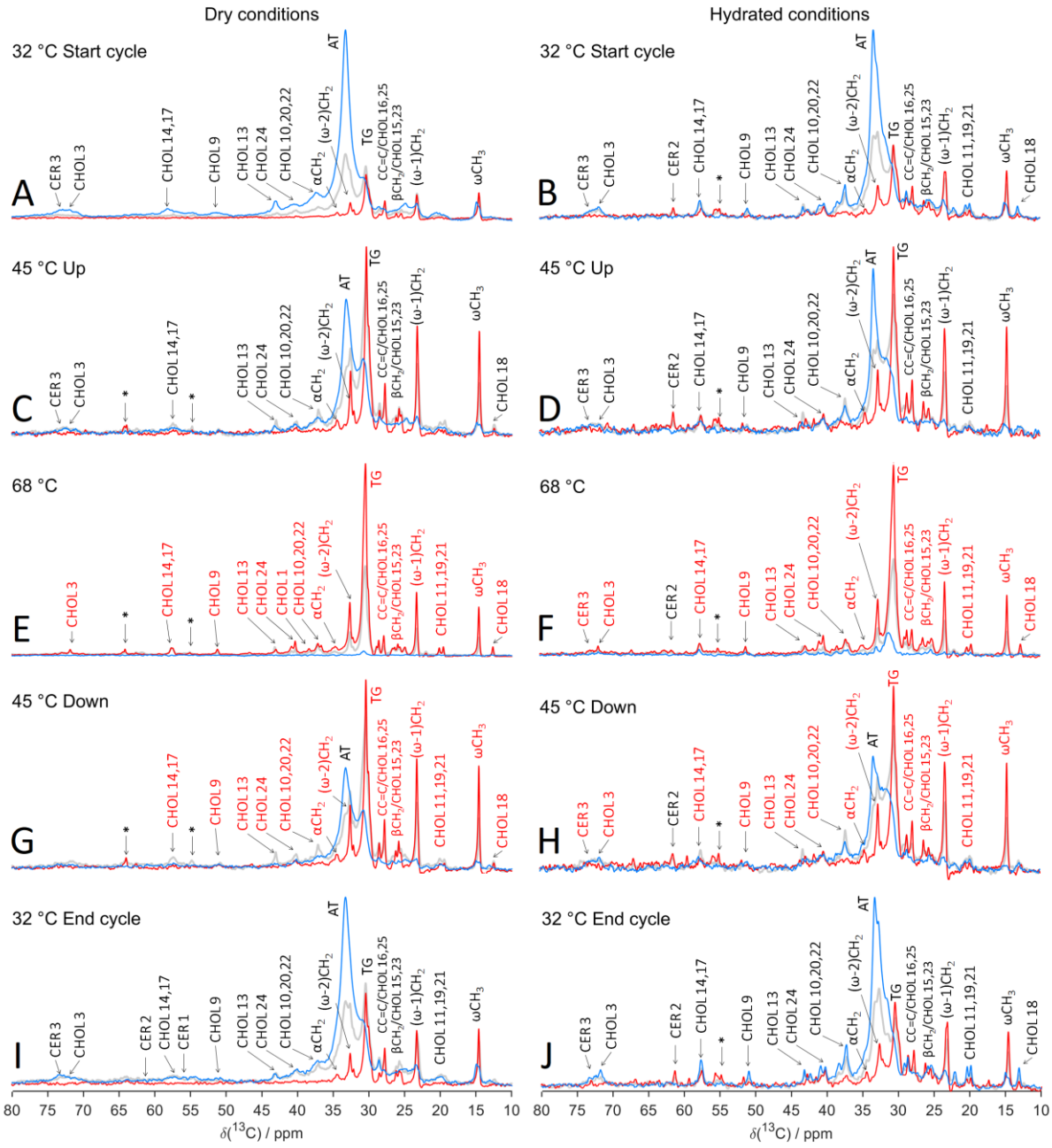

Figure 4.10: DP (grey), CP (blue) and INEPT (red) ^{13}C spectra of extracted lipids in dry and fully hydrated conditions. A—B corresponds the spectra measured at 32 ˚C (beginning of cycle), C—D at 45 ˚C (increasing temperature), E—F at 68 ˚C (height of temperature cycle), G—H 45 ˚C (decreasing temperature) and I—J at 32 ˚C (end of cycle). Labels in red indicate a greater INEPT:CP ratio using the end of the cycle temperature as reference. Peak marked with * could not be assigned.

At 45 ˚C, **1)** INEPT to CP intensity ratio has increased, indicating that the acyl chains are transitioning to a fluid state. The presence of AT and TG peaks indicates a coexistence of a solid and an isotropic fluid phase, which has been observed in previous studies [43]. **2)** INEPT to CP intensity ratio corresponding to CHOL is increasing for most of its carbons, hinting at a higher mobility of the molecule with increasing temperature. **3)** CER carbons corresponding to the headgroup (Figure 4.11 C) more rigid compared to the rest of the molecule, this is evident in the downfield region (Figure 4.12 C).

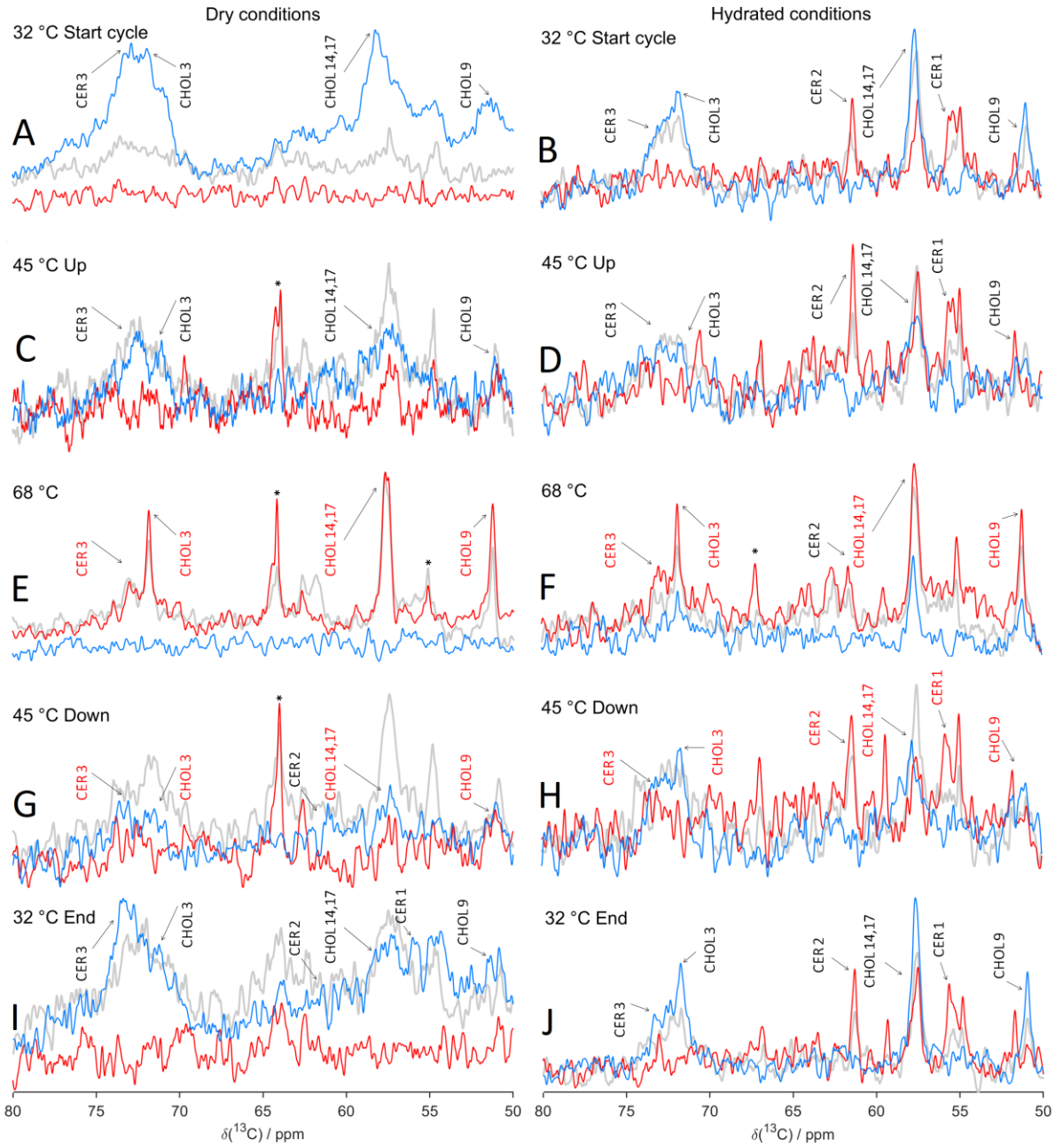

Figure 4.11: DP (grey), CP (blue) and INEPT (red) ^{13}C spectra of extracted lipids in dry and fully hydrated conditions, zoomed in between 50—80 ppm. A—B corresponds the spectra measured at 32 ˚C (beginning of cycle), C—D at 45 ˚C (increasing temperature), E—F at 68 ˚C (height of temperature cycle), G—H 45 ˚C (decreasing temperature) and I—J at 32 ˚C (end of cycle). Labels in red indicate a greater INEPT:CP ratio using the end of the cycle temperature as reference.

68 ˚C Maximum temperature

Figures 4.10, **4.11**, **4.12 E** shows the maximum temperature 68 ˚C. **1), 2)** and **3)** There is mainly INEPT signal contribution except for a broad peak (TG). The abundance of INEPT signal throughout the whole ppm spectrum, and very low/no CP signal, indicates the existence of an isotropic. This suggests that at lower temperatures, the lipid chains are AT consequently rigid, and at 68 ˚C they have melted and are TG and mobile, implying a solid to liquid phase transition. This is consistent with previous PT ss-NMR studies on with SC lipids at varying water contents (24, 37, 50 wt%) [30].

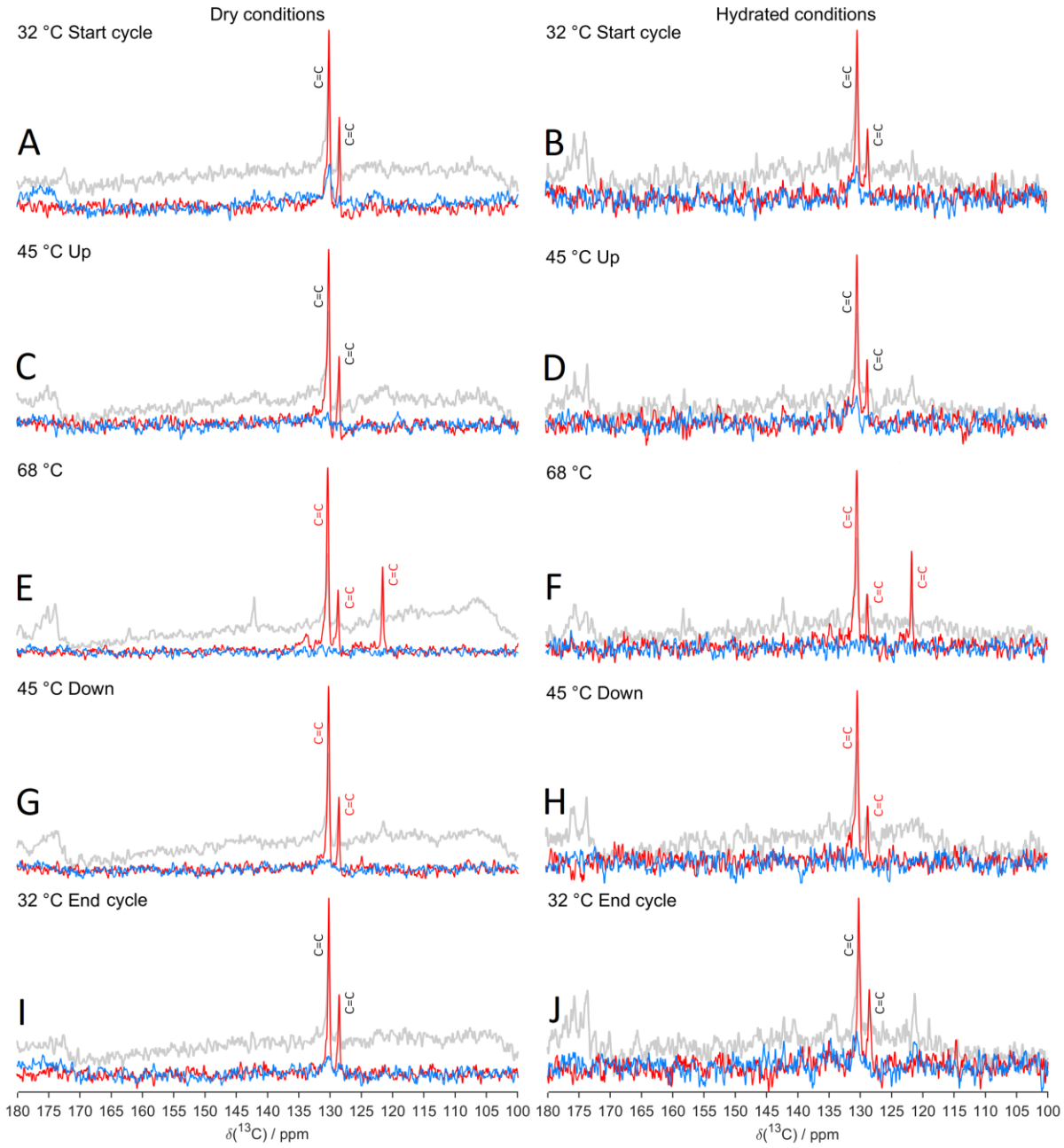

Figure 4.12: DP (grey), CP (blue) and INEPT (red) ^{13}C spectra of extracted lipids in dry and fully hydrated conditions, 100—180 ppm. A—B corresponds the spectra measured at 32 ˚C (beginning of cycle), C—D at 45 ˚C (increasing temperature), E—F at 68 ˚C (height of temperature cycle), G—H 45 ˚C (decreasing temperature) and I—J at 32 ˚C (end of cycle). Labels in red indicate a greater INEPT:CP ratio using the end of the cycle temperature as reference.

45 ˚C Downscan

Figures 4.10, 4.11, **4.12 G** shows the sample after at 45 ˚C downscan. **1)** Acyl chains display both INEPT to CP intensity ratio. Furthermore, the AT peak has reappeared, and the spectra indicate co-existence of AT and TG chain conformations. **2)** Most CHOL peaks display a high INEPT to CP intensity ratio, confirming that cholesterol has been dissolved in fluid lipids. **3)** CER headgroup carbons display very low intensity of both CP and INEPT, indicating an intermediate regime. CERs peaks corresponding to chain segments close to the headgroup are still in a mobile state. The conjugated double bonds (Figure 4.12 G), which likely are part of ceramides [47] are also in a mobile state. Overall the structure is in both a rigid and a fluid state.

32 ˚C End cycle

Figures 4.10, 4.11, **4.12 I**, show the end of the cycle 32 ˚C. **1)** The INEPT to CP intensity ratio has decreased, indicating that the methylene groups have an AT conformation. INEPT to CP intensity ratio is clearly higher compared to the corresponding sample at 32 ˚C before the heating cycle. **2)** CHOL has low INEPT to CP intensity ratio, suggesting that the structure is in a rigid state. Again, the INEPT to CP intensity ratio is higher after the heating cycle. **3)** CER peaks in the headgroup and in chain segments close to the headgroup (Figure 4.11 I, Figure 4.10 I respectively) all display a lower INEPT to CP intensity ratio compared to 45 ˚C, indicating that the headgroups are following the trend displayed by CHOL and acyl chains: a higher portion of CER headgroups are in the rigid structure. Finally, the conjugated double bonds (Figure 4.12 I) give rise to high INEPT signal, implying mobile isotropic segments. The majority of the double bonds, assumed to be part of CER molecules [47], and the combined results thereby suggest strong variation in molecular mobility within the very same ceramide molecules. This has also been shown for SC model lipid systems [47].

Summary dry conditions

The main fraction of dry SC lipids melt when the temperature is increased to 68 ˚C. Cooling down the lipids, gradually causes them to become rigid once again. At 68 ˚C the lipid chains display isotropic reorientation, as evidenced by the disappearance of the AT peak: the lipids have melted. Cooling down the sample reverses the fluid phase back into a coexistence of phases, as seen by the AT peak reappearing. Here, however, we can observe that the lipids are in a more mobile state as compared to the beginning of the temperature cycle.

It is noted that there is a difference in INEPT to CP intensity ratio in dry conditions before and after the heating cycle. This could likely have an origin in the dissolution of cholesterol in the lipid mixture. At 68 ˚C, when cholesterol is dissolved in the mixture, there is a different composition of the lipid system, where cholesterol disturbs the close packing of the chain, while it may also induce mobility. This can be seen in the SAXS spectra (Figure 4.7 A), where at 68 ˚C cholesterol reflections disappear and the reflections corresponding to LPP and SPP can be resolved after 68 ˚C, when cholesterol has dissolved [48]. Another likely explanation for the INEPT to CP intensity ratio before and after the heating cycle could be equilibration effects. For a solid sample, like SC lipids, equilibration takes a long time. This could mean that the system, at the time of measuring, has not yet reached equilibrium.

It can also observed that the lipids are in a more mobile state as compared to the beginning of the temperature cycle.

Effects of hydration on extracted lipids

32 ˚C Start cycle & 45 ˚C upscan

Figures 4.10, **4.11**, **4.12 B** and **D** show the lipids at the start of the cycle and the first upscan. **1)** the AT peak dominates over the spectra. INEPT to CP intensity ratio is higher compared to the sample in dry conditions, indicating that there is a larger acyl chain population in a fluid

phase. **2)** CP relative intensities of CHOL are higher compared to dry conditions, indicating that CHOL is less mobile at this temperature when the sample has been fully hydrated. **3)** CER peaks follow the same trend as the acyl chain and CHOL peaks and display a higher INEPT to CP intensity ratio.

At 45 °C. **1)** Acyl chain peaks all display a higher relative INEPT intensity which indicates that the methylene groups have an increasing isotropic reorientation. **2)** CHOL carbons also display high INEPT to CP intensity ratio, which increases gradually with temperature, indicative of higher mobility. **3)** CER peaks corresponding to the head and to chain segments close to the headgroup display a higher relative INEPT signal intensity. Overall the INEPT to CP intensity ratio increases with temperature, indicating that increasing temperature induces mobility on the lipids.

68 ˚C Maximum temperature

Figures 4.10, **4.11**, **4.12 F** shows the spectra at 68 ˚C. **1), 2)** and **3)** There is an overall predominance of INEPT signal throughout the whole spectra. However, there is small contribution from CP signal for the TG peak, indicative of an anisotropic structure. The AT peak is still visible, albeit with a low relative intensity. This indicates the presence of a small amount of lipids that are not melted. These data can be compared to previous PT ss-NMR studies of intact SC, which showed that for water contents of 37 wt% and 50 wt% no corresponding CP signal could be resolved in the crowded NMR spectra at 60 ˚C.

45 ˚C Downscan

Figures 4.10, 4.11, **4.12 H** shows the sample 45 ˚C after the sample has been heated to 68 ˚C**. 1)** Similar to what was described for the sample in dry conditions, the relative CP intensity of the AT peak has increased after the sample has cooled down from 68 ˚C, while the TG peak still dominates over the spectra, indicating a coexistence of rigid and mobile phases at 45 ˚C. **2)** CHOL carbons exhibit some INEPT signal contribution indicating that at least a fraction of CHOL is present in a mobile state. **3)** CER peaks follow the same trend as CHOL carbons, displaying some mobility.

32 ˚C End cycle

Figures 4.10, 4.11, **4.12 J**, show the end of the cycle, 32 ˚C. **1)** Both INEPT and CP signals are detected, but the INEPT signal is much lower compared to 45 ˚C and 68 ˚C, the AT peak is dominating, indicating that the main part of the sample is in a rigid state but still containing a small fraction of fluid lipid segments. **2)** INEPT to CP intensity ratio of CHOL peaks has decreased compared to 45 ˚C and 68 ˚C, suggesting increased rigidity. **3)** Most peaks from CER carbons show a lower INEPT to CP intensity ratio compared to higher temperatures, with the exception of CER C2. This suggest that the headgroup and chain segments close to the headgroup are in a more rigid phase as the temperature decreases, but still showing signs of mobility. The conjugated double bonds corresponding to the tail segment [47] of the molecule show mobility (Figure 4.12 J).

Summary fully hydrated conditions

As observed with the sample in dry conditions, the lipids undergo a transition between solid and fluid phases. The overall effect is reversible, but there are still clear differences for the sample at 45 ˚C and 68 ˚C, when comparing the same temperatures before and after heating. The possible explanation could be the dissolution of cholesterol in the lipid mixture, and/or effects caused by the sample not reaching equilibrium, as was the case during dry conditions. When reaching 68 ˚C, in hydrated conditions, there is still an AT peak visible. There is INEPT signal contribution throughout the whole spectral regime at even the lowest temperatures, especially evident at the end of the temperature cycle.

Dry vs fully hydrated conditions

At 32 ˚C, relevant skin temperature, hydration induces mobility, which is most apparent for cholesterol and ceramides. This trend is seen before and after the heating cycle. At 45 ˚C, the same conclusion can be reached. At 68 ˚C, the addition of water to the sample leads to the appearance of a CP signal. This may be related to the formation of an anisotropic liquid crystalline structure. The sample in dry conditions is likely an isotropic fluid, whereas the addition of water can lead to the formation of self-assembled structures (liquid crystalline phases) [10].

Conclusion

In these PT ss-NMR studies, it has been observed that lipids, upon being subjected to gradually increasing temperatures, mobility is induced. This isotropic reorientation is exhibited at different degrees depending on the type of lipid, with the acyl chains displaying the highest mobility. In dry conditions, high temperatures also cause the entirety of the sample to melt. Lowering the temperature causes the lipids to become gradually more rigid, with coexistence of fluid and rigid phases. Returning to the lowest temperature induces rigidity upon the lipids, albeit this time, the sample shows increased mobility compared to the beginning at 32 ˚C, as evidenced by the relatively higher INEPT to CP intensity ratio throughout the 10—80 ppm regime.

When comparing the lipids sample at the same temperature, before and after the heating cycle, clear differences were observed, in both dry and fully hydrated conditions. These differences in signal intensity could have an explanation in that cholesterol, at high temperatures, it dissolves in the lipid mixture, consequently the lipid system will have a different composition. Here, cholesterol disturbs the close packing of the chain, and it may also induce mobility. This effect, which can be observed in the SAXS spectra (Figure 4.7 A), where at the highest temperature and after the heating cycle, Bragg reflections corresponding to cholesterol are not seen, while the LPP and SPP higher order reflections can be resolved (seen as more defined peaks), after cholesterol has dissolved [48].

When fully hydrated, at the lowest temperatures there is a sign of mobility as evidenced by the higher relative INEPT intensity of the hydrophobic chain segments, CHOL carbons and the headgroup region of ceramides (especially visible at the end of the temperature cycle, 32 ˚C). At 32 ˚C and 45 ˚C, there is generally higher mobility in hydrated samples for CER and CHOL.

At 68 ˚C, the appearance of CP signal indicates the formation of an anisotropic structure. Formation of liquid crystalline structure is also expected is water is added to a melt of amphiphilic lipid molecules [10].

4.3.3 Capillary cell to study lipid formation at an interface

During this project, the development and improvement of a suitable sample preparation method for the capillary technique used to study self-assembly in a water gradient was undertaken. The purpose of the sample preparation was to form an oriented lipid film at the edge of the capillary cell which was to be observed under the microscope. Solvents such as water and organic solvents were tested.

Different approaches were taken, such as the use of high temperatures, sonication of samples, freeze-thaw cycles, and lipid droplet fusing at the interface. The first two approaches were successful. The lipids were dispersed in water, heated to 80 ˚C for ~3 h, and then sonicated at high power, yielding a clear solution of lipids that was suitable for analysis under the microscope. There were several complications with the organic solvents and fuse of interfacial lipid droplets approaches:

- pentane had too low surface tension: when the pentane solution reached the tip, the solution with lipids flowed out of the cell too easily (Figure 4.13 C)
- hexane was too difficult to handle, and not suitable to work with under the microscope
- chloroform dissolved the optical glue

On the other hand, the advantage with solvent methods was that it took almost no time to form a lipid film at the edge of the capillary cell. One main drawback with the approach using lipids dispersed in water is that it takes a long time to form a lipid film of acceptable dimensions (3-4 days). There is also risk of forming cholesterol crystals (Figure 4.13 B). However, crystallization of cholesterol was circumvented by the use of temperature higher than RT and high RH.

Results & conclusion

The lipid films obtained from water dispersion can be seen in Figure 4.13. The capillary cells were put between cross polarizers filters in order to distinguish between isotropic and birefringent samples.

The image seen in Figure 4.13 A, was obtained after 3 days at 45 °C and 99% RH, for 0°. It can be observed that the sample is birefringent at this angle (the lipids at the interface are seen as bright), which is consistent with a lamellar structure. The sample was also analyzed at 45°, however this was done under different temperature and RH conditions, not allowing a direct comparison.

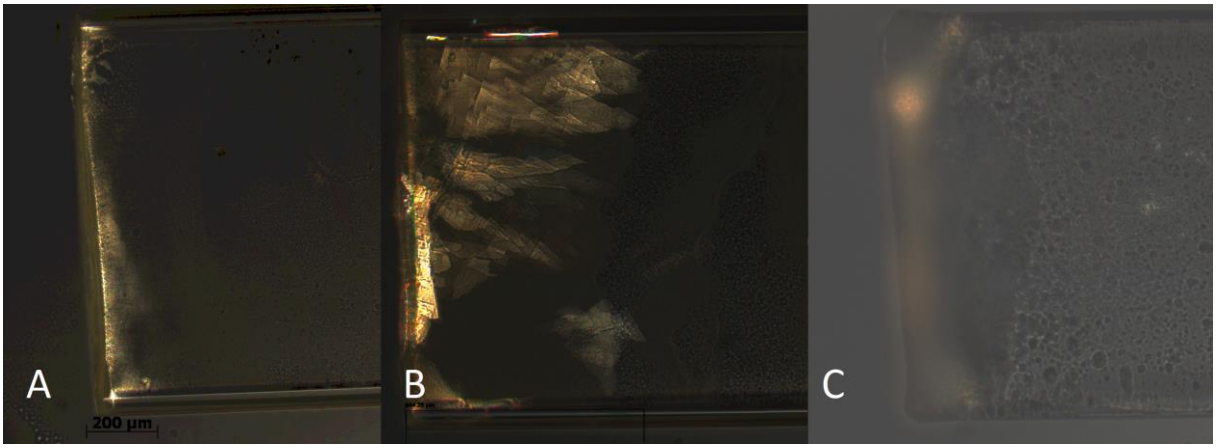

Figure 4.13: A shows a magnification at 0° of the edge of the capillary cell with a ~200 µm wide lipid film forming at the interface. **B** shows cholesterol crystals forming at room temperature and RH. **C** shows the lipid film forming when a pentane solution is used, here the lipid-pentane solution flowed out of the cell, possibly due to low surface tension, this happened in almost all attempts with pentane. Zoom: 10x.

5. CONCLUSIONS

In this study a new lipid extraction method was tested and further modified. This new modified method, Method III, was chosen based on ^{13}C NMR analysis (Figure 4.3). The properties of SC were also studied by rebuilding its NMR spectra using individual ^{13}C NMR spectra of corneocytes and lipids. It was shown that by combining the spectra of the two, it was possible to reconstruct the spectra of SC, indicating that the properties of corneocytes and lipids are close to additive, and their behavior in terms of molecular mobility does not change significantly when they are separated (Figure 4.6).

Further investigation of the molecular mobility of lipids with PT ss-NMR showed that the entirety of the lipid sample melts upon reaching 68 °C in dry conditions. However, in fully hydrated conditions, there was still an amount of lipids displaying anisotropic reorientations. The lipids in dry and fully hydrated conditions at the end of the temperature cycle at 32 ˚C. In particular hydration has a strong effect on the mobility of cholesterol and ceramide headgroups.

The structural properties of the SC lipids were studied with X-ray scattering, where SAXS showed that the lipids in both dry and fully hydrated conditions and after being subjected to a temperature cycle, attain order, in form of defined Bragg peaks, which made it possible to detect LPP and SPP, with corresponding higher order reflections. The spacings of these phases differed to LPP and SPP values found in the literature for similar systems, which could be due to the composition of the extracted lipids. WAXS showed the characteristic hexagonal chain packing peaks, as well as liquid phase peaks for porcine SC lipids. Hydration does not seem to affect the lateral chain packing and it showed only small effect on the lamellar phases (Figure 4.7 D).

Particularly evident in scattering experiments was the effect of that the heating cycle has on the sample. The lipids sample is annealed and becomes more ordered. The heating cycle also causes cholesterol to dissolve in the lipid mixture, which means that long and/or short periodicity

phases can form without the need for complicated procedures taken by other groups [17, 40, 46]. To ensure equilibrium is reached, longer equilibration times after the maximum temperature step are advisable.

It is worth noting that for scattering and NMR experiments, these were performed one time, it would therefore also be advisable to repeat the experiments (also in different conditions, particularly for intact SC) to confirm the findings observed in this study.

ACKNOWLEDGEMENTS

First I would like to thank my supervisor, Prof. Emma Sparr, and my co-supervisor Dr. Enamul H. Mojumdar:

Emma: I am extremely grateful to you for giving me the chance to work in this project, and the internship I did last year. Seeing how you work, and how involved you are with the people working with you, inspired me to do my best, and I hope you're not disappointed. For all the knowledge you provide (and not just to me), thank you .

Enamul: You've taught me a lot during these months, and the months during the internship, and whether at MaU or at KC, you were always ready to help. Sincerely, thank you.

I would also like to thank Dr. Quoc Dat Pham: thank you Dat for answering the endless string of questions I bombarded you with during all these months.

Lastly, I would like to thanks the people who allowed my project, and all projects at fkem to be running.

REFERENCES

[1] Kezic S, Jakasa I (2016) Filaggrin and Skin Barrier Function. Skin barrier function. Basel: Karger. 1.

[2] Forslind B, Lindberg M (2004) Structure and Function of the Skin Barrier: An Introduction. Skin, hair, and nails. Basel: Dekker. 11.

[3] van Smeden J, Bouwstra J (2016) Stratum Corneum Lipids: Their Role for the Skin Barrier Function in Healthy Subjects and Atopic Dermatitis Patients. Basel: Karger. 9.

[4] Wertz P, Madison K, Downing D (1989). Covalently Bound Lipids of Human Stratum Corneum. J Invest Dermatol 92: 109—111.

[5] Elias P, Feingold K (2001) Does the tail wag the dog? Role of the barrier in the pathogenesis of inflammatory dermatoses and therapeutic implications. Arch Dermatol 137: 1079—1081.

[6] Sparr E, Engström S (2004) Lipid Phase Behavior: A Basis for an Understanding Of Membrane Structure and Function. Skin, hair, and nails. Basel: Dekker. 25.

[7] Weerheim A, Ponec M (2001) Determination of stratum corneum lipid profile by tape stripping in combination with high-performance thin-layer chromatography. Arch Dermatol Res 293: 191—199.

[8] Elias P (1996) The Stratum Corneum Revisited. J Dermatol 23: 756—768.

[9] Sparr E, Engström S (2004) Lipid Phase Behavior: A Basis for an Understanding Of Membrane Structure and Function. Skin, hair, and nails. Basel: Dekker. 26.

[10] Evans D, Wennerström H (1999) The colloidal domain where physics, chemistry, biology and technology meet (2nd ed). Danvers: Wiley-VCH. 9—10, 306—307 .

[11] Berg J, Tymoczko J, Gatto G, Stryer L (2015) Biochemistry (8th ed). NY: W.H. Freeman. 344, 772.

[12] van Smeden J, Hoppel L, van der Heijden R, Hankemeier T, Vreeken R, Bouwstra J (2011) LC/MS analysis of stratum corneum lipids: ceramide profiling and discovery. J Lipid Res 52: 1211—1221.

[13] Bouwstra J, Ponec M (2006) The skin barrier in healthy and diseased state. Biochimica et Biophysica Acta 1758: 2080—2095.

[14] Norlén L, Nicander I, Lundsjö A, Cronholm T, Forslind B (1998) A new HPLC-based method for the quantitative analysis of inner stratum corneum lipids with special reference to the free fatty acid fraction. Arch Dermatol Res 290: 508—516.

[15] van Smeden J, Boiten W, Hankemeier T, Rissmann R, Bouwstra J, Vreeken R (2014) Combined LC/MS-platform for analysis of all major stratum corneum lipids, and the profiling of skin substitutes. Biochim Biophys Acta. Molecular and Cell Biology of Lipids 1841: 70—79.

[16] Epstein E (1981) Steroid Sulfatase, X-Linked Ichthyosis, and Stratum Corneum Cell Cohesion. Arch Dermatol 117: 761.

[17] Bouwstra J, Gooris G, Bras W, Downing D (1995) Lipid organization in pig stratum corneum. J Lipid Res 36: 685—695.

[18] Lindblom G, Rilfors L (1989) Cubic phases and isotropic structures formed by membrane lipids — possible biological relevance. Biochim Biophys Acta. Reviews on Biomembranes 988: 221—256.

[19] Tanford C (1981) The Hydrophobic effect: Formation of micelles and biological membranes. J Chem Educ 58: A246.
[20] Evans D, Wennerström H (1999) The colloidal domain where physics, chemistry, biology and technology meet (2nd ed). Danvers: Wiley-VCH. 14—15.
[21] Holmberg K, Kronberg B, Lindman B, Jönsson B (2002) Surfactants and polymers in aqueous solutions. West Sussex: Wiley & Sons. 54.
[22] Luckey M (2014) Membrane Structural Biology (2nd ed). NY: Cambridge University Press. 31.
[23] Lee A (2004) How lipids affect the activities of integral membrane proteins. Biochim Biophys Acta 1666: 62–-87.
[24] Evans D, Wennerström H (1999) The colloidal domain where physics, chemistry, biology and technology meet (2nd ed). Danvers: Wiley-VCH. 306—307.
[25] Andersson J (2018) Self-Assembly in Lipid-Protein Systems. Doctoral Dissertation. Lund University. 5.
[26] Sparr E, Engström S (2004) Lipid Phase Behavior: A Basis for an Understanding Of Membrane Structure and Function. Skin, hair, and nails. Basel: Dekker. 35—36.
[27] Levitt M (2015) Spin dynamics. Chichester: Wiley. 14.
[28] Nowacka A (2012) Polarization transfer solid-state NMR for studying soft matter: From surfactants to the stratum corneum. Doctoral Dissertation. Lund University. 22.
[29] Laws D, Bitter H, Jerschow A (2002)Solid-State NMR Spectroscopic Methods in Chemistry. Angew Chem 41: 3096—3129.
[30] Björklund S, Nowacka A, Bouwstra J, Sparr E, Topgaard D (2013) Characterization of Stratum Corneum Molecular Dynamics by Natural-Abundance ^{13}C Solid-State NMR. PLoS ONE 8: e61889.
[31] Als-Nielsen J, McMorrow D (2011) Elements of modern X-ray physics. West Sussex: Wiley. 5.
[32] Schnablegger H, Singh Y (2017) The SAXS Guide Getting acquainted with the principles (3rd ed). Austria: Anton Paar GmbH. 19.
[33] Fox M (2010) Optical properties of solids (2nd ed). Wiltshire: Oxford University Press. 48.
[34] Boiten W, Absalah S, Vreeken R, Bouwstra J, van Smeden J (2016) Quantitative analysis of ceramides using a novel lipidomics approach with three dimensional response modelling. Biochim Biophys Acta. Molecular and Cell Biology of Lipids 1861: 1652—1661.
[35] Bligh E, Dyer W (1959) A rapid method of total lipid extraction and purification. Can J Biochem Phys 37: 911—917.
[36] Schaefer H, Redelmeier T (1996) Composition and structure of the stratum corneum. Skin barrier: principles of percutaneous absorption. Basel: Karger. 43–86.
[37] Wertz P, Downing D (1987) Covalently bound ω-hydroxyacylsphingosine in the stratum corneum. Biochim Biophys Acta. Lipids and Lipid Metabolism 917: 108—111.
[38] Doucet J, Potter A, Baltenneck C, Domanov Y (2014) Micron-scale assessment of molecular lipid organization in human stratum corneum using microprobe X-ray diffraction. J Lipid Res. 55: 2380—2388.
[40] Bouwstra J, Gooris G, van der Spek J, Bras S (1991) Structural investigations of human stratum corneum by small-angle X-ray scattering. J Invest Dermatol 97: 1005—1012.

[41] Bouwstra J, Gooris G, Dubbelaar F, Ponec M (2001) Phase behavior of lipid mixtures based on human ceramides: coexistence of crystalline and liquid phases. J Lipid Res 42: 1759—1770.
[42] Björklund S, Nowacka A, Bouwstra J, Sparr E, Topgaard D (2013) Characterization of Stratum Corneum Molecular Dynamics by Natural-Abundance ^{13}C Solid-State NMR. PLoS ONE 8: e61889. [Online] https://doi.org/10.1371/journal.pone.0061889.s001. (accessed Aug 22)
[43] Chen X, Kwak S, Lafleur M, Bloom M, Kitson N, Thewalt J (2007) Fatty Acids Influence "Solid" Phase Formation in Models of Stratum Corneum Intercellular Membranes. Langmuir 23: 5548—5556.
[44] Pappas A (2009) Epidermal surface lipids. Dermatoendrocrinol 1: 72—76.
[45] Wertz P, Downing D (1983) Ceramides of pig epidermis: structure determination. J Lipid Res 24: 759—765.
[46] White S, Mirejovsky D, King G (1988) Structure of lamellar lipid domains and corneocyte envelopes of murine stratum corneum. Biochemistry 27: 3725—3732.
[47] Pham Q, Mojumdar E, Gooris G, Bouwstra J, Sparr E, Topgaard D (2018) Solid and fluid segments within the same molecule of stratum corneum ceramide lipid. QRB-D 51 E7: 1—9
[48] Mouritsen O, Bagatolli L (2016). Life - as a matter of fat (2nd ed.). Berlin: Springer. Chapter 9.4.

APPENDIX

Table A1 shows the peak assignment performed by Björklund et al [30] used to identify the lipid peaks.

Table A.1. Peak assignment done by Börklund et al of intact pig stratum corneum (SC).

δ (ppm)	**Molecule**	**Segment**
11.6	Ill	Cδ
12.7	Cholesterol	C18
13.3	Cholesterol	C18
14.6	Aliphatic	ωCH_3
16.1	Ill	C_γ
17.6	Ala	C_β
19.6	Cholesterol	C21
20.1	Cholesterol	C19
20.5	Cholesterol	C11
19.7-20.1	Val, Thr	C_γ
22.0-22.2	Cholesterol	C26 / C27
22.1	Leu / Lys	Cδ2 / Cγ
23.3	Aliphatic	$(\omega\text{-}1)CH_2$
23.4	Leu	Cδ1
25.0-26.8	Aliphatic, Cholesterol	βCH_2, C15 / C23
25.5	Leu, Arg, Ill	C_γ
27.4-28.0	Glu, Gln, Lys	C_β
27.9-29.0	Aliphatic, Cholesterol	**C**C=C, C25 / C16
29.2	Arg, His	C_β
29.5-31.2	Aliphatic	$(CH_2)_n$
30.5	Val	C_β
32.0-32.7	Aliphatic	$(\omega\text{-}2)CH_2$
32.3	Glu, Gln / Lys	C_γ / C_δ
34.8-36.0	Aliphatic	αCH_2
36.7	Cholesterol	C10
37.0	Tyr, Ill, Phe	C_β
37.3	Cholesterol	C22
37.5	Cholesterol	C20
37.6-37.9	Asn, Asp	C_β
38.4	Cholesterol	C1
40.4	Cholesterol	C24
40.6	Leu / Lys	C_β / C_ε
40.9	Cholesterol	C12
41.8	Arg	C_δ
42.8	Cholesterol	C4
43.4	Cholesterol	C13
43.7	Gly	C_α
≈50-60	All amino acid residues (except Gly)	C_α
51.2	Cholesterol	C9

56.3	Ceramides	C1
56.7	Ser	C_α
62.3	Ceramides	C2
62.4	Ser	C_β
68.1	Thr	C_β
72.0	Cholesterol	C3
73.2	Ceramides	C3
116.6	Tyr	C_ε
118.6	His	C_δ
121.4	Cholesterol	C6
121.7	Ceramides	C=C
127.9	Tyr / Phe	C_γ / C_ζ
128.7	Ceramides	C=C
129.6	Tyr / Phe	C_δ / C_ε
130.2	Phe	C_δ
130.5	Ceramides	C=C
131.5	His	C_γ
134.0	Ceramides	C=C
136.8	Phe	C_γ
137.7	His	C_ε
142	Cholesterol	C5
155.9	Tyr	C_ζ
158.0	Arg	C_ζ
172-182	Amino acid residues and SC lipids	C=O

Table A2 below summarizes the amounts of SC obtained. Skin batch II consisted of SC strips that had not been properly soaked in trypsin, which made the separation with tweezers difficult. This was fixed by excluding them from batch I and soaking them in additional trypsin.

Table A.2. Amount of SC obtained after dermatoming, washing, drying overnight. Batch II was the "difficult" batch. Batch I and II came from 25 ears, batch III came from 16 ears.

Skin Batch	m SC (g)
I	2,101
II	0,606
III	2,568

Table A3 below shows the amount of lipids obtained after each extraction performed

Table A.3. Amount of lipids obtained and remaining COR after each extraction procedure.

Lipid Extraction Batch	Method	m lipids (mg)	m SC (g)	m COR (g)
I a	Method II	53.8	1.065	0.6930
I b	Method III	78.0		
II	Method III	138	1.027	0.6646
III	Method III	132	1.085	0.6919

Figure A1 shows the 13C NMR spectra of n-heptane, a remaining solvent that contaminated the COR sample. It was removed after extensive washing with methanol and Milli-Q.

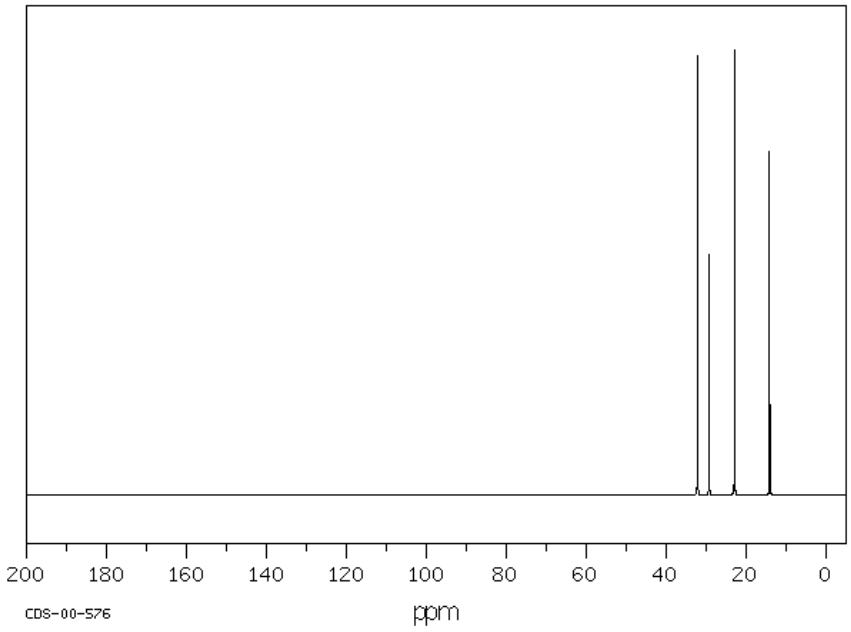

Figure A.1: ^{13}C NMR spectrum of *n*-heptane in $CDCl_3$**.** SDBS No.: 2396 from https://sdbs.db.aist.go.jp

Figure A2 shows the 13C NMR spectra of washed corneocytes.

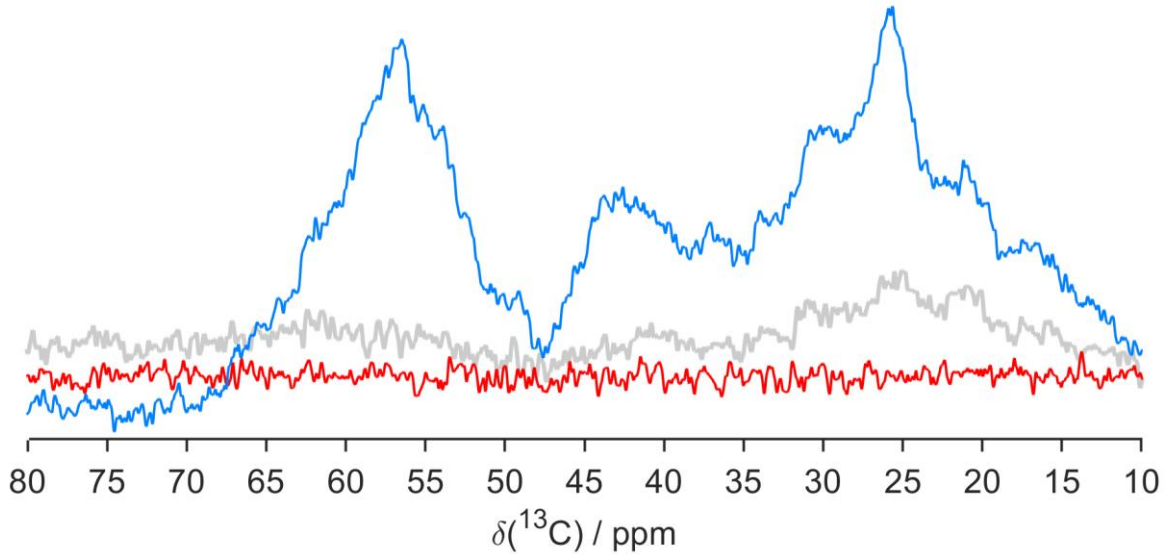

Figure A.2: **^{13}C** NMR spectra of COR after extensive washing with methanol, ethanol, Milli-Q**.** Sample was measured at 32 ˚C and in dry conditions.

Figure A3 shows the background SAXS spectra for Kapton film

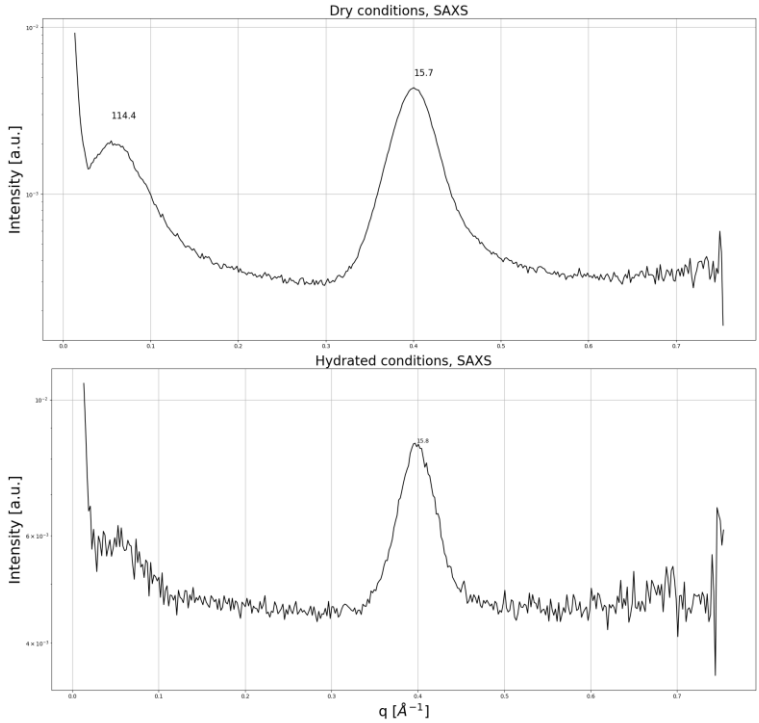

Figure A.3:SAXS pattern for Kapton film used throughout the scattering measurements in dry and hydrated conditions (water in excess contained between two sheets of Kapton film). Scattering patterns were obtained at 32 °C

Figure A4 shows the background WAXS spectra for Kapton film.

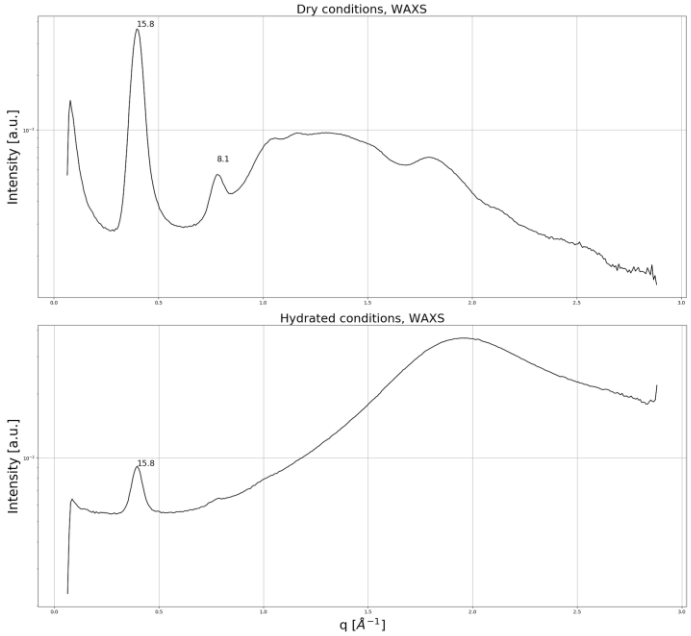

Figure A.4:WAXS pattern for Kapton film used throughout the scattering measurements in dry and hydrated conditions (water in excess contained between two sheets of Kapton film). Scattering patterns were obtained at 32 °C

Figure A5 shows the SAXS spectra of lipids in dry conditions used to fit the higher orders of LPP and SPP.

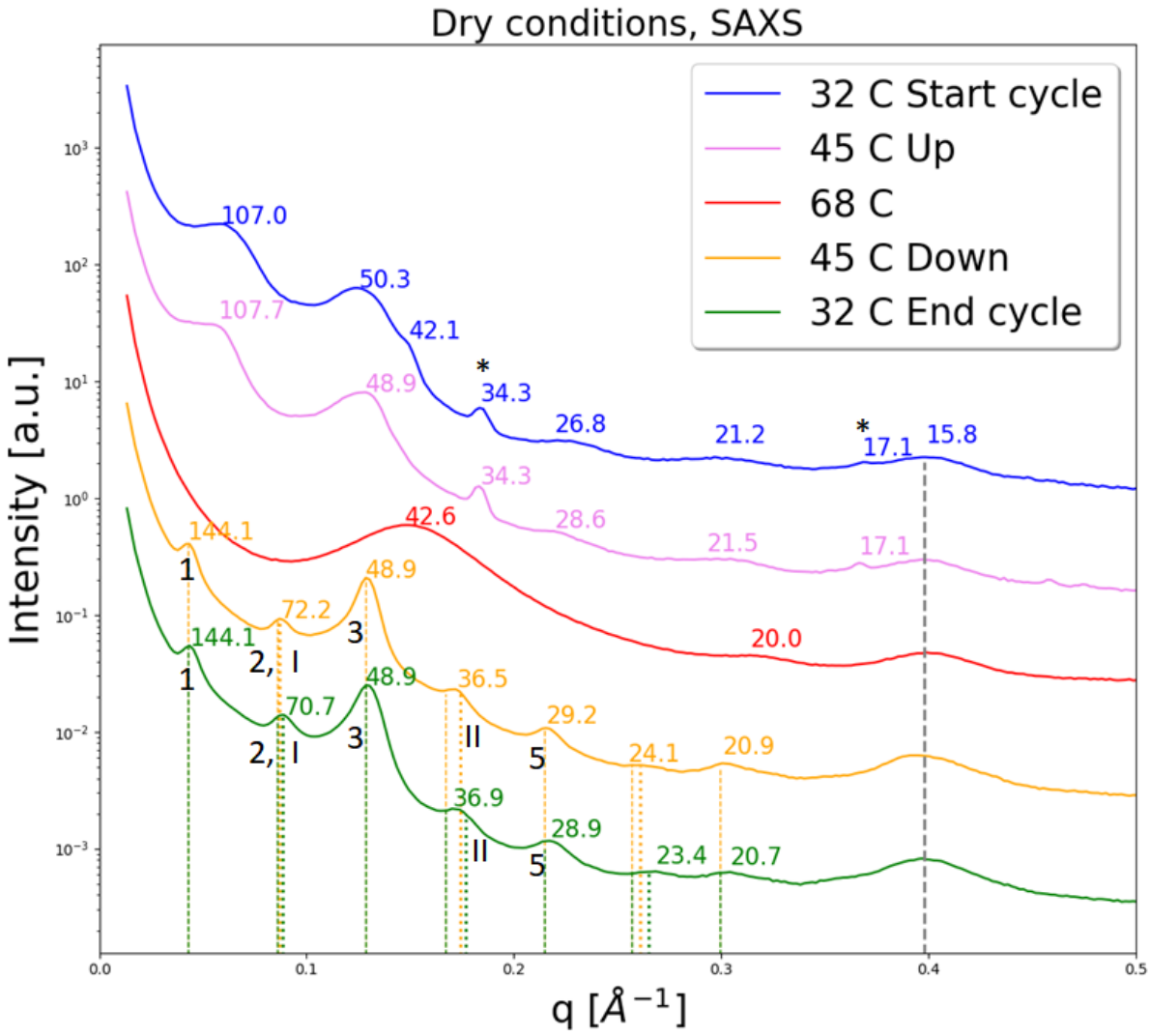

Figure A.5:SAXS pattern for lipids sample. Dotted lines represent LPP higher orders, thick dots represent SPP higher orders. 3 used as reference peak for LPP, I (roman numeral) used as reference for SPP. Assigning the peaks was a compromise between the fitting the parallel line (dotted line or thick dots) and the peak given by the peak-finding algorithm (Python).

Figure A6 shows the SAXS spectra of lipids in hydrated conditions used to fit the higher orders of LPP and SPP.

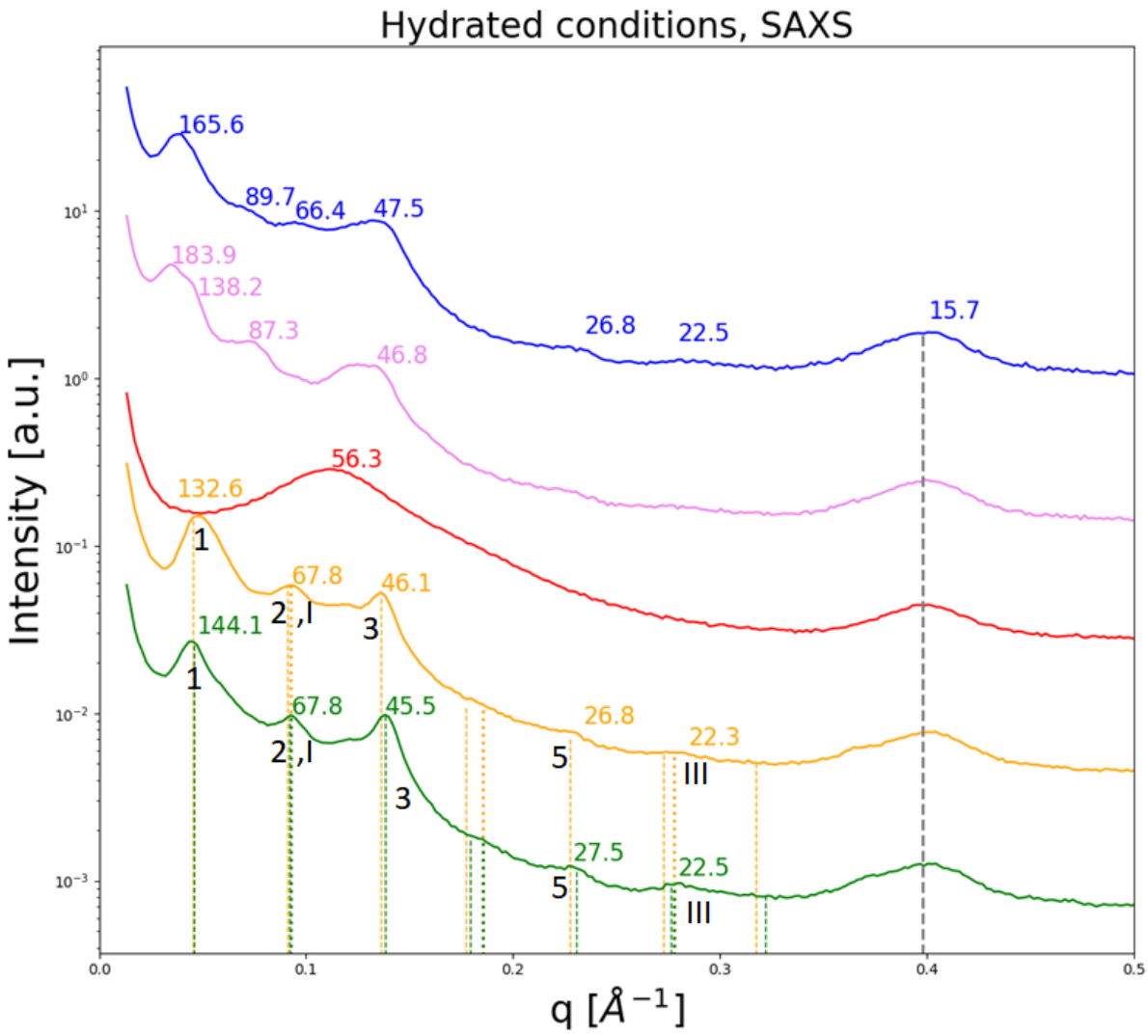

Figure A.6 SAXS pattern for lipids sample in hydrated conditions. Dotted lines represent LPP higher orders, thick dots represent SPP higher orders. 3 used as reference peak for LPP, I (roman numeral) used as reference for SPP. Assigning the peaks was a compromise between the fitting the parallel line (dotted line or thick dots) and the peak given by the peak-finding algorithm (Python).